

# We are IntechOpen, the world's leading publisher of Open Access books Built by scientists, for scientists

4,800

Open access books available

122,000

International authors and editors

135M

Downloads

Our authors are among the

154

Countries delivered to

TOP 1%

most cited scientists

12.2%

Contributors from top 500 universities



WEB OF SCIENCE™

Selection of our books indexed in the Book Citation Index  
in Web of Science™ Core Collection (BKCI)

Interested in publishing with us?  
Contact [book.department@intechopen.com](mailto:book.department@intechopen.com)

Numbers displayed above are based on latest data collected.  
For more information visit [www.intechopen.com](http://www.intechopen.com)



# Application of meta-material concepts

Ho-Yong Kim<sup>1</sup> and Hong-Min Lee<sup>2</sup>  
<sup>1</sup>*ACE antenna,*  
<sup>2</sup>*Kyonggi University*  
*Korea*

## 1. Introduction

Wave propagation in suppositional material was first analyzed by Victor Vesalago in 1968. Suppositional material is characterised by negative permittivity and negative permeability material properties. Under these conditions, phase velocity propagates in opposite direction to group velocity. This phenomenon is referred to as “backward wave” propagation. The realization of backward wave propagation using SRR (Split Ring Resonator) and TW (Thin Wire) was considered by Pendry in 2000. Since then, these electrical structures have been studied extensively and are referred to as meta-material structures. In this chapter we will analyze meta-material concepts using transmission line theory proposed by Caloz and Itho and propose effective materials for realising these concepts. We propose a novel NPLH (Near Pure Left Handed) transmission line concept to reduce RH (Right Handed) characteristics and realize compact small antenna designs using meta-material concepts. In addition we consider enhancing radiation pattern gain of an antenna using FSS (Frequency Selective Surface) and AMC (Artificial Magnetic Conductor). Finally the possibility of realising negative permittivity using EM shielding of concrete block is considered.

## 2. Means of meta-material concepts

The RH and LH transmission lines are shown in Fig. 1.

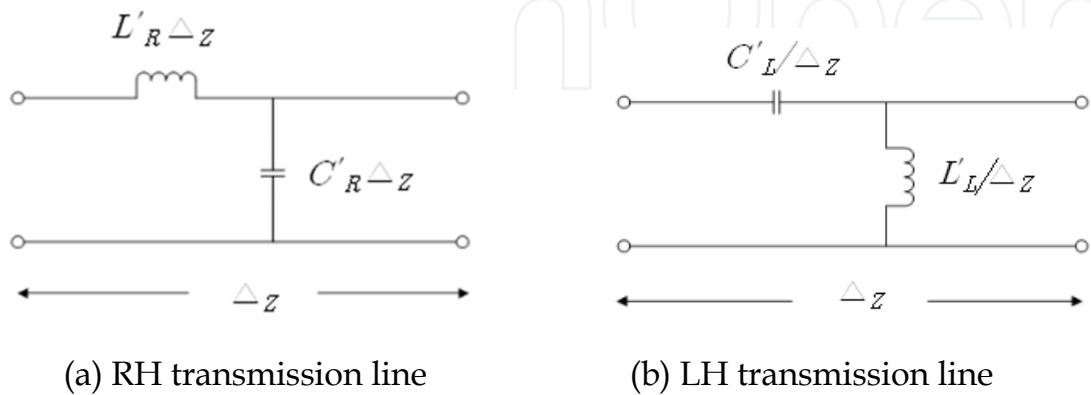


Fig. 1. RH and LH transmission lines

The RH (Right Handed) transmission line consists of serial inductance( $L'_R$ ) and parallel capacitance ( $C'_R$ ). The serial inductance ( $L'_R\Delta z$ ) and prallel capacitance ( $C'_R\Delta z$ ) per unit lenth are as following equatiion.

$$C'_R\Delta z = \epsilon_0\epsilon_r \frac{w}{d}(F/m)$$
$$L'_R\Delta z = \mu_0\mu_r \frac{d}{w}(H/m)$$

(1)

Where, the w is width of transmission line, the d is thickness of substrate.

We will consider negative permittivity and negative permeability in transmission line. The serial inductance ( $L'_R\Delta z$ ) and parallel capacitance ( $B_{meta}$ ) are replaced as negative reactance( $X_{meta}$ ), which are expressed as following equation.

$$X_{meta}=-j\omega|L'_R\Delta z| = -j\frac{1}{\omega C_{eff}}$$
$$B_{meta}=-j\omega|C'_R\Delta z| = -j\frac{1}{\omega L_{eff}}$$

(2)

We know that electrical performance of  $L'_R$  and  $C'_R$  are changed into serial capacitance( $C'_L$ ) and prallel inductance( $L'_L$ ) in negative permeability and negative permittivity material. If we added serial capacitance on normal transmission line, the transmission line with serial capacitance exhibits similar transmission line characteristic using ENG (Epsilon Negative) material. Also, if we use parallel inductance on normal transmission line, the transmission line with parallel inductance express transmission line using MNG (Mu Negative) material. Therefore, we know that the metamaterial concepts can be realized by electrical loading structures, which are gap of microstrip line, via and so on. The applications of meta-material are shown in Fig. 2. The SNG (Single Negative) materials include ENG material and MNG material. The DNG (Double Negative) material has negative permittivity and negative permeability simultaneously. We will deal with small antenna, CRLH (Composite Right/Left Handed) transmission line, FSS and AMC

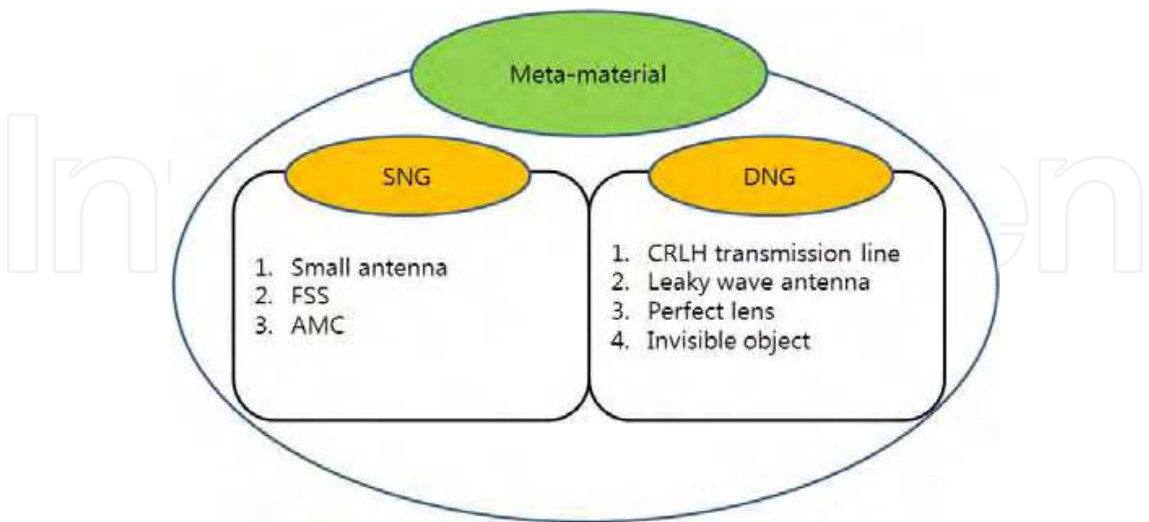


Fig. 2. The applications of meta-material concepts

3. NPLH transmission line

3.1 Introduction

Synthesis of meta-material structures has been investigated using various approaches. Amongst these approaches, the transmission line approach has been used to verify backward wave characteristics of LH transmission lines.

The pure LH (PLH) transmission line can be realized by a unit cell, which is composed of a series capacitor and a parallel inductor and must satisfy effectively homogeneous conditions. However it is difficult to realize an ideal pure LH transmission line, due to generation of parasitic RH (Right Handed) element characteristics of the transmission line which consist of a series inductor and parallel capacitor. A composite Right/ Left Handed (CRLH) transmission line structure concept is therefore used.

A balanced CRLH transmission line structure shows band pass characteristics. The LH dispersion range is below center frequency of pass band and the RH dispersion range is above the center frequency. The LH range is however typically narrow because it is limited by RH parasitic elements.

In this section we use a planar parallel plate structure to realise a NPLH transmission line with reduced RH element characteristics. Radiation loss calculations of the LH range is provided and the structure is optimized using CST MWS.

3.2 Analysis of transmission line

The CRLH transmission line and the unit cell of LH transmission line are shown in Fig. 3. The realization of LH transmission line based on microstrip line can't avoid parasitic RH components such as  $C'_R$  and  $L'_R$ . However, if the  $C_R$  and  $L_R$  approximate open state and short state, The Pure LH line can be realized. Consequently, in this paragraph, we replace ground plates as ground lines to reduce  $C'_R$ . Also, the signal line is composed by contiuous capacitive plates for minimization of  $L'_R$ .

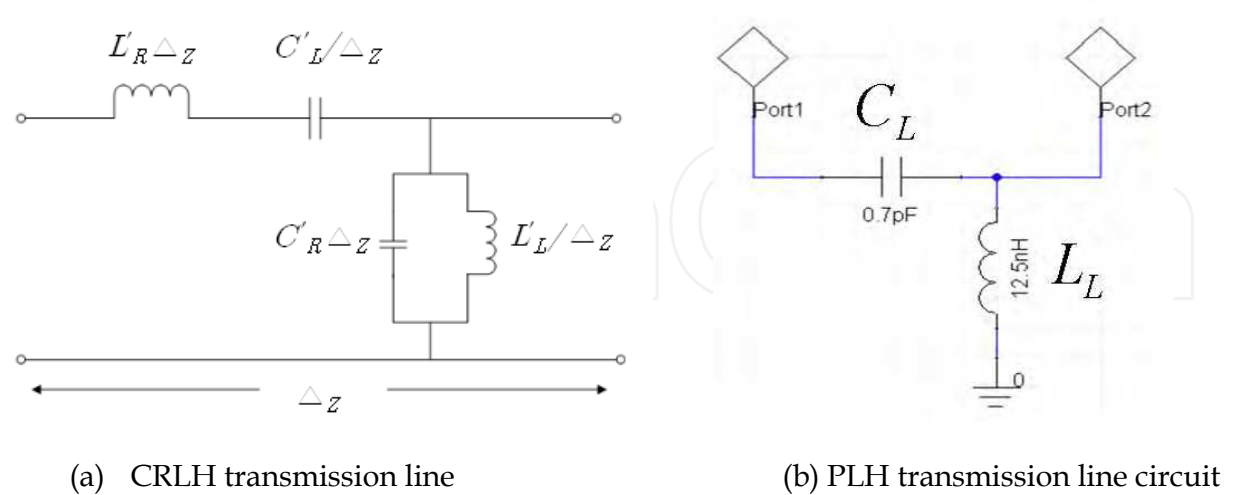


Fig. 3. The CRLH transmission line and the unit cell of LH transmission line

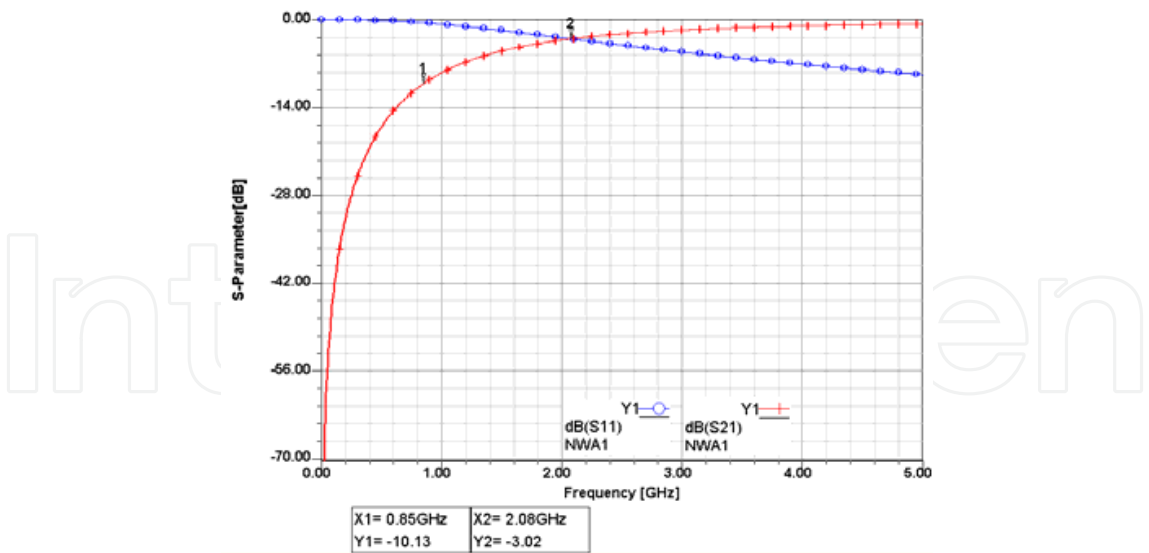


Fig. 4. The S-parameter of PLH transmission line circuit

The PLH transmission line circuit is shown in Fig. 3(b). A large series capacitance of PLH transmission line is needed for applying matched condition in low frequency band, but it is difficult to realize  $C_L$  because it needs very large dimesion. To reduce of physical size of PLH transmission line, the equivalentnt circuit of proposed transmission line is provided in unmatched conditin. The S-parameter of PLH transmission line circuit is shown in Fig. 4. The cutoff frequency( $\omega_{CLH}$ ) of PLH transmission line has equation as following

$$\omega_{CLH} = 0.5 \frac{1}{\sqrt{C_L L_L}} \tag{3}$$

The  $\omega_{CLH}$  is about 850MHz. The pass band starts at 2.08GHz. The equivalentnt circuit of 2 cell-NPLH characteristic is shown in Fig. 5. Near the port 2, the  $C_R$  is added in order to achieve the reciprocal characteristic between 1-port and 2-port. Most CRLH transmission line has a weak point in analysis using circuit simulation. Specially, the important factors of PLH transmission line are phase and radiation loss. The additional components, which are generated by coaxial probe, must be considered for analysis of phase in PLH transmission line. The coaxial feed section, which consists of  $C_f$  and  $L_f$ , is added at equivalentnt circuit of 2 cells-PLH transmission line.

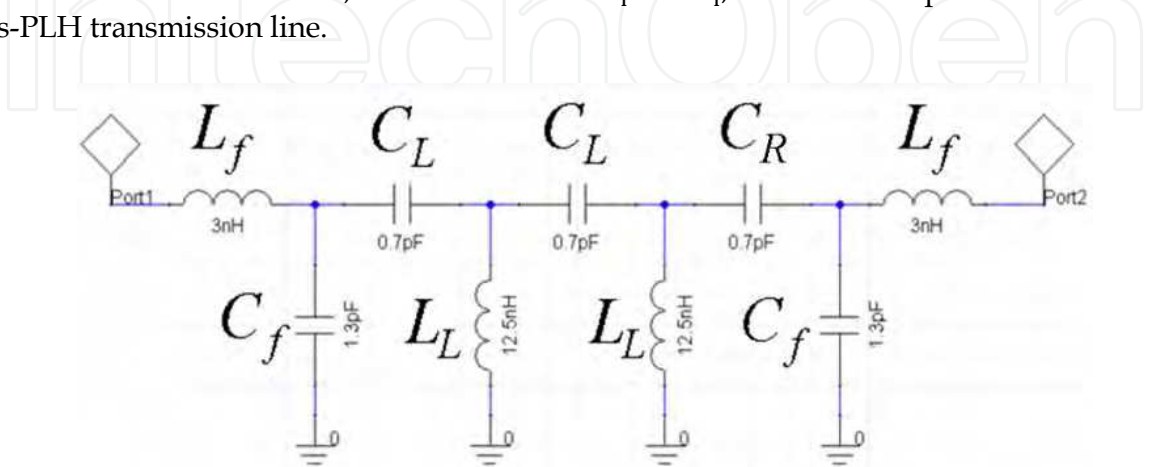


Fig. 5. The equivalentnt circuit of 2-cells NPLH transmission line

When the coaxial feed section is applied at equivalent circuit, two differences are shown. First is a change of pass band range and second is a start point of phase. The S-parameter of NPLH transmission line equivalent circuit is shown in Fig. 6. The cutoff frequency is 0.92GHz. The resonance frequencies are 1GHz and 2.05GHz. The transmission bandwidth (over -3dB)of the transmission coefficient is 1.08GHz.

The loci of transmission coefficient of equivalent circuit are shown in Fig. 7. It is important result to realize NPLH transmission line physically, the phases of NPLH transmission line must coincide with the phases of equivalent circuit each frequency.

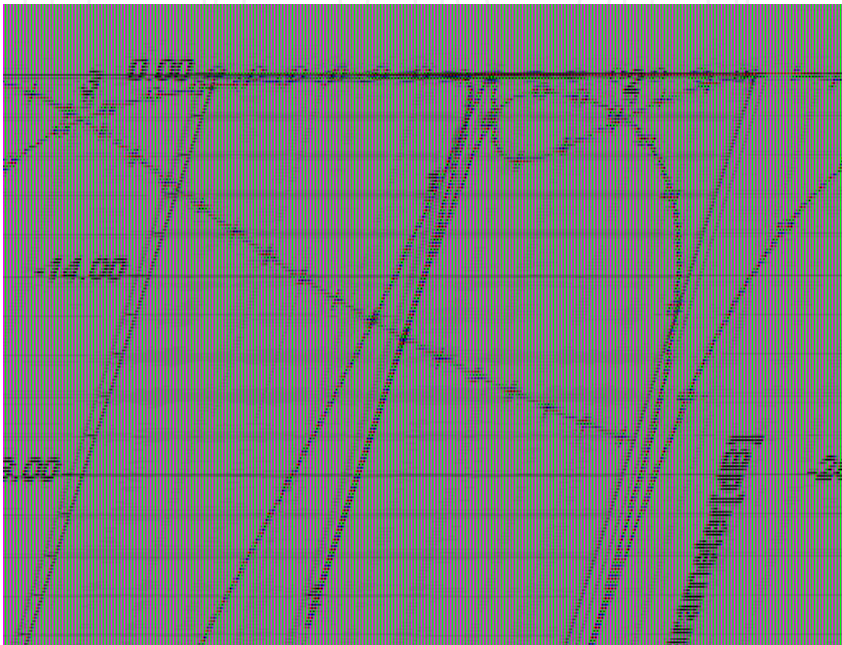


Fig. 6. The S-parameter of NPLH transmission line equivalent circuit

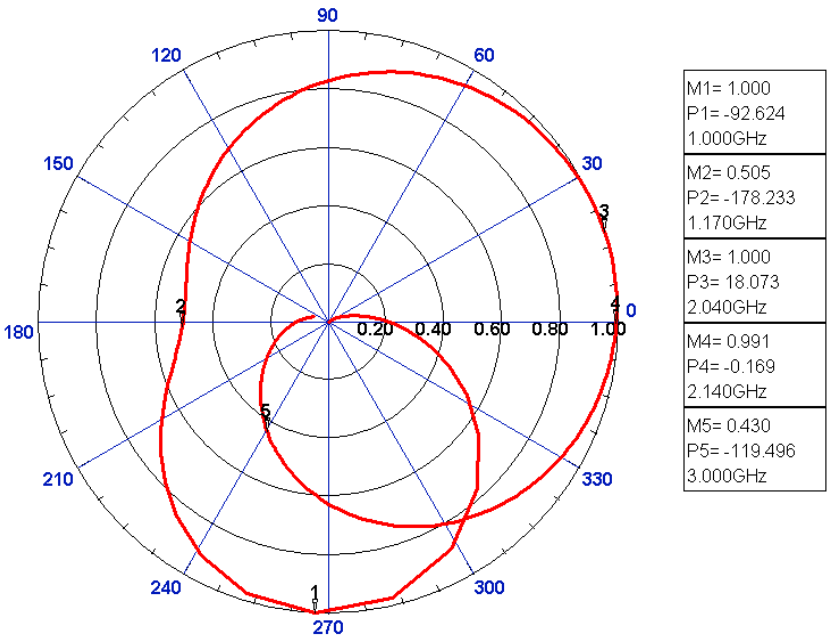


Fig. 7. The loci of transmission coefficient at equivalent circuit



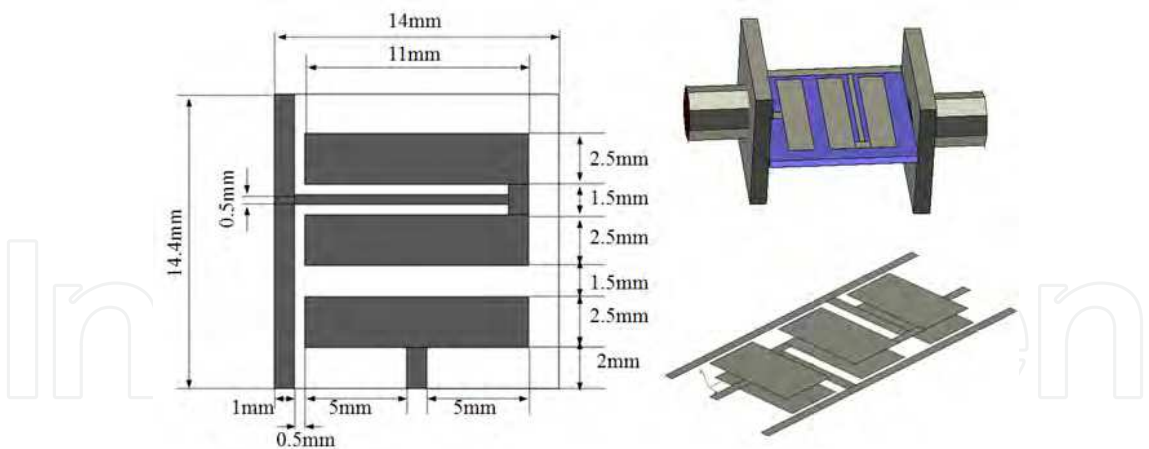


Fig. 8. The geometry of proposed NPLH transmission line

3.3 Simulated and experimental results

The geometry of proposed NPLH transmission line is shown in Fig. 8. The proposed NPLH transmission line consists of MIM (Metal-Insulate-Metal) capacitor and parallel inductor line. The physical size of componetns is calculated by distributed elements design. The ground plane of proposed NPLH transmission line is simplified as line structure for reduction of parallel capacitor between ground and signal line. Also, to reduce series inductance, the transition line among cells is very short length. The substrate of proposed NPLH transmission line is Teflon, which is relative permittivity constant is 2.17. The S-parameter using 3D filed simulation is shown in Fig. 9. There is similarity between S-parameter results of 3D field simulation and equivalent circuit. The resonance frequencies are 1.17GHz and 2.15GHz. The pass bandwidth (over -3dB) of transmission coefficient is 0.94GHz. Also loci of transmission coefficients between equivalent circuit and 3D field simulation are very similar. The loci of transmission coefficient using 3D filed simulation are shown in Fig. 10. The proposed NPLH transmission line achieves near pure left handed characteristic.

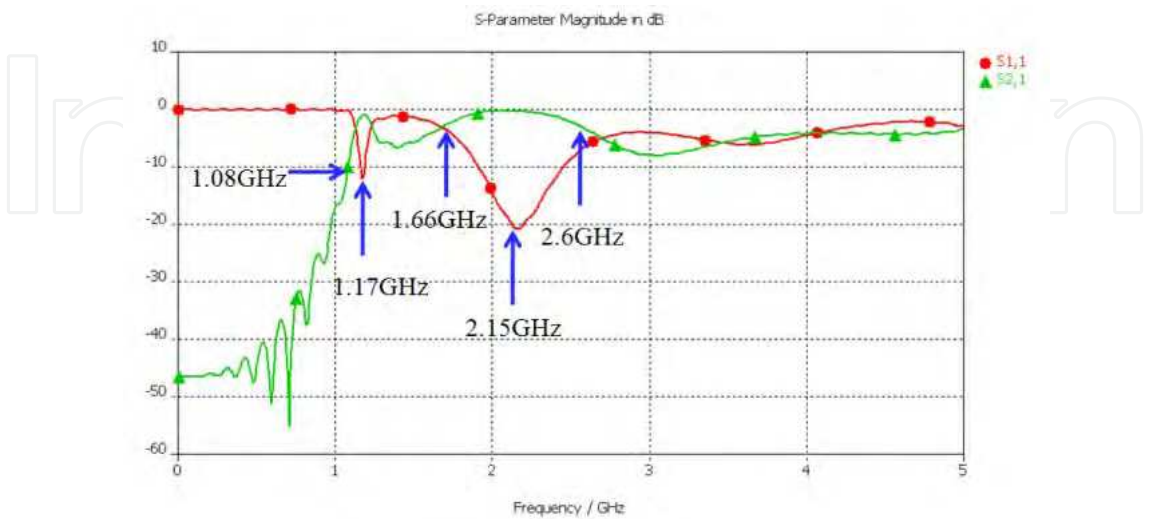


Fig. 9. The S-parameter using 3D filed simulation

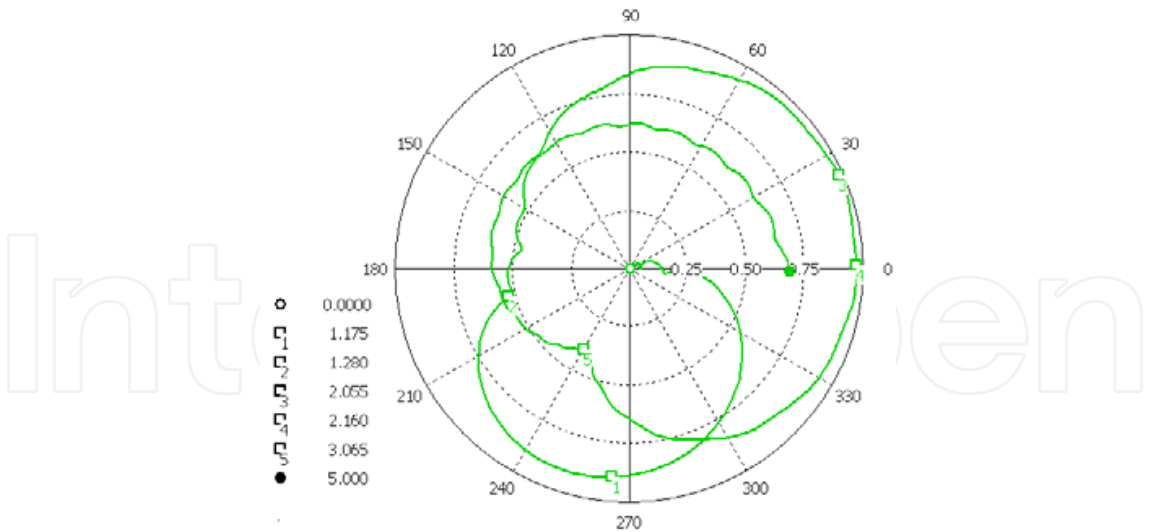


Fig. 10. The loci of transmission coefficient using 3D filed simulation

The backward wave characteristic is shown at frequency range below 3GHz. Due to limitation of a distributed elements design at frequency range over 3GHz The normal E-field distrigution at 2.15GHz is shon in Fig. 11.

The insertion loss is related with a radiation loss. In case of proposed NPLH transmission line, if the total power is 100%, the transmission power is calculated as following two equations.

$$S_{21r}[\%] = 100 - 100 * 10^{S_{11}[\text{dB}]/10}, \qquad S_{21i}[\%] = 100 - 100 * 10^{S_{21}[\text{dB}]/10} \qquad (4)$$

Where,  $S_{21r}$  and  $S_{21i}$  are calculated at reflection coefficient and insertion loss respectively. The radiation power( $P_{\text{rad}}$ )is expected as following equation

$$P_{\text{rad}}[\%] = S_{21r}[\%] - S_{21i}[\%] \qquad (5)$$

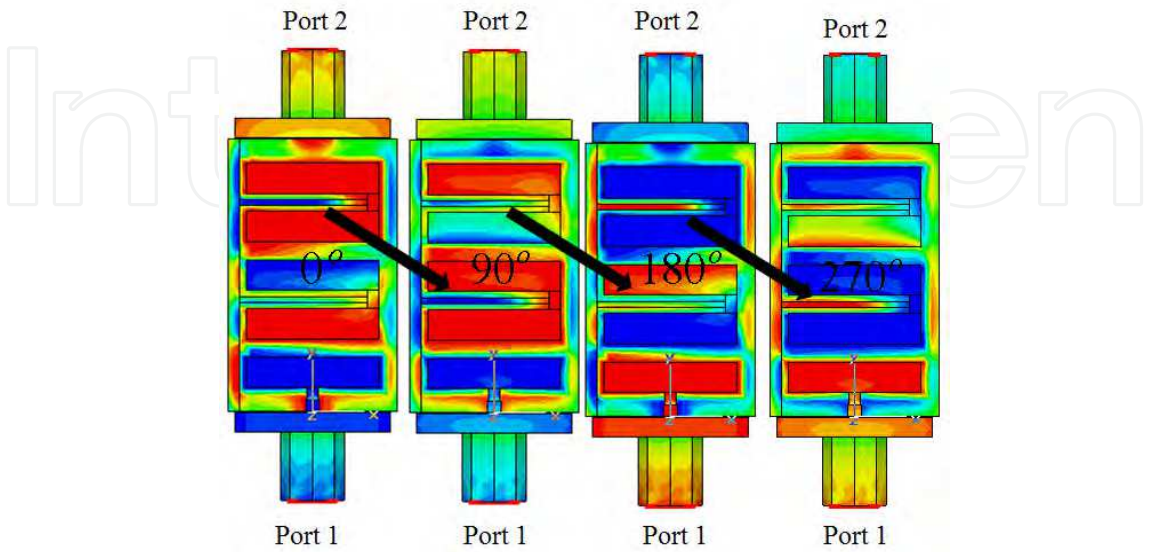


Fig. 11. The normal E-field distribution at 2.15GHz



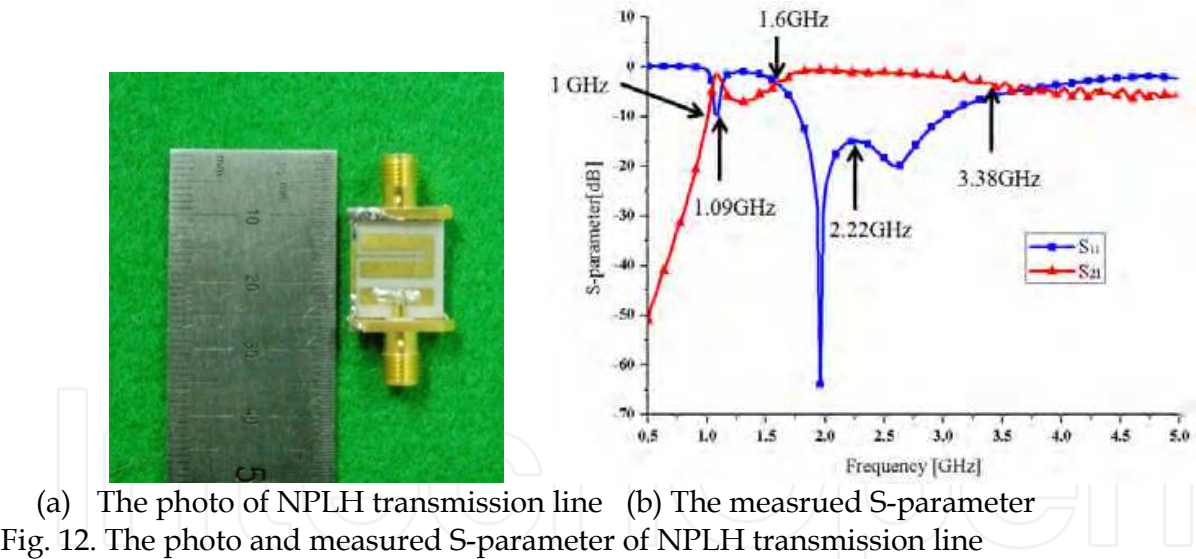
The  $P_{rad}$ , which is calculated at 2.6GHz, is about 33%. There are very similar results between  $P_{rad}[\%]$  and radiation efficiency of 3D simulation result. The radiation losses at each frequencies are shown in Table1.

The photo and measured S-parameter of fabricated NPLH transmission line is shown in Fig. 12. The pass bandwidth of transmission coefficient(over=3dB) is 1.78GHz.

The NPLH transmission line using prallel plate structure is proposed. The proposed structure shows backward wave characteristics which a PLH transmission line should have. The provided equivalent circuit model of a NPLH transmission line simulation results are similar with and ideal PLH transmission line characteristics. Also, The radiation loss which is deliverated by  $S_{11}$  and  $S_{21}$ . We understand realization method of near pure left handed transmission line using distributed elements and means of meta-material concepts in paragraph. We will study compact antenna using metamaterial concepts in next paragraph.

| Frequency(GHz) | Radiation loss(%) | Frequency(GHz) | Radiation loss(%) |
|----------------|-------------------|----------------|-------------------|
| 1.7            | 0.21              | 2.2            | 6.18              |
| 1.8            | 0.43              | 2.3            | 10.73             |
| 1.9            | 0.96              | 2.4            | 17.16             |
| 2              | 1.82              | 2.5            | 24.53             |
| 2.1            | 3.39              | 2.6            | 31.16             |

Table 1. Radiation losses of NPLH transmission line



4. The compact antenna using meta-material concepts

4.1 Introduction

The electrically small antenna is defined as  $ka < 1$  where  $k$  is the wave number and  $a$  is the maximum length of antenna. For electrically small antennas efficiency, gain, impedance bandwidth and quality factor ( $Q$ ) vary as a function of maximum length of antenna. Miniaturization of an antenna typically results in narrower impedance bandwidth, higher  $Q$  and lower gain. The reduction of defects of small antennas is the main consideration in design of electrically small antennas.

Recently an EESA (Efficient Electrically Small Antenna) was proposed by Richard W.

| Capacitance (unit: pF) |      | Inductance (unit: nH) |    | Resistance (unit: $\Omega$ ) |       |       |       |
|------------------------|------|-----------------------|----|------------------------------|-------|-------|-------|
| $C_f$                  | 1.2  | $L_m$                 | 4  | $R_1$                        | 40.7k | $R_2$ | 0.637 |
| $C_m$                  | 0.15 | $L_g$                 | 36 | $R_3$                        | 81k   | $R_4$ | 0.779 |

Table 2. The values of equivalent circuit elements

Ziolkowski in 2006 and simulated using HFSS. The EESA was achieved using a spherical shell of SNG (Single Negative) or DNG (Double Negative) materials. The SNG and DNG material characteristics are realized using electrical structures. These techniques will be applied for miniaturization of an antenna in this section.

4.2 The equivalent circuit of small antenna using ENG material concepts

The concept of proposed antenna is shown in Fig. 13. The equivalent circuit of proposed small antenna is shown in Fig. 14. Generally the small monopole antenna has a high capacitance due to very short length. Therefore the inductance loading is necessary for the impedance matching of a small monopole antenna. The impedance matching can be achieved by negative permittivity meta-material structure, which is equivalent parallel inductance in this paragraph.

The two port equivalent circuit of proposed antenna is realized by open condition. The  $C_f$  is a capacitance of coaxial feed and feeding pad. The  $L_m$  is an inductance of monopole antenna and coaxial feed. The  $C_m$  is a capacitance among monopole antenna, ground and negative permittivity meta-material structure.

We find that parallel inductance is operated as negative permittivity in first paragraph. The  $L_g$  is an inductance of negative permittivity meta-material structure in effective material. The values of equivalent circuit elements are shown in table 2. The resonance frequency of equivalent circuit is 2.04GHz

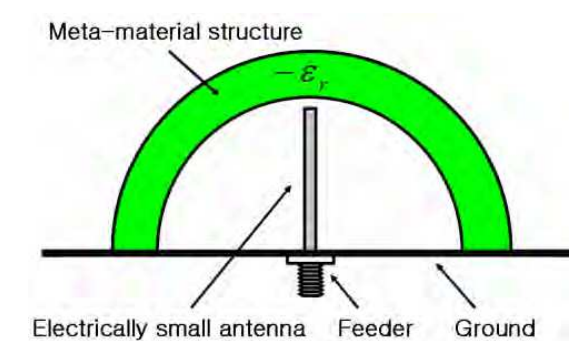


Fig. 13. The concept of proposed antenna

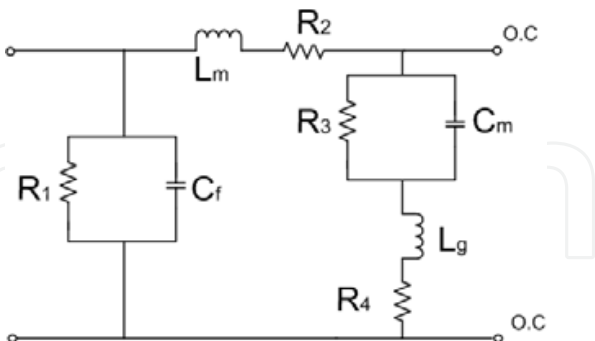


Fig. 14. The equivalent circuit

4.3 The realization and experiment of small antenna using equivalent circuit

The idea and geometry of the proposed antenna are shown in Fig 15. The substrate is FR4 ( $\epsilon_r$ : 4.9) and the subtreate thickness is 0.8mm. The proposed antenna is excited by a coaxial feed structure. The geoemtry is obtained by calculated passive components.

We consider thin wire in free space. The length of thin wire is about  $0.5 \lambda$  for resonance condition. The resonated thin wire has high inductive characteristic at lower band of

resonance frequency. This factor can be applied for negative permittivity in proposed structure. But we have to reduce length of thin wire and apply shorted thin wire for small antenna. The shorted thin wire is alternated as defected ground structure, which is called meta-material structure in this geometry. The inductance of coaxial feed and monopole are insufficiency for resonance of antenna. Therefore, the additional inductance is needed and realized by meta-material structure.

The simulated characteristics of proposed antenna are shown in Fig. 16. The resonance frequency and the impedance bandwidth ( $VSRW \leq 2$ ) are 2.035GHz and 155MHz at 3D field simulated results. We find that loci of impedance are very similar between circuit simulation and 3D filed simulation. The geometry is corresponded with equivalent circuit. The field distribution of proposed antenna is shown in Fig. 17(a). The normal E-field is concentrated between monopole and negative permittivity meta-material structure.

We see that surface currents are flowed on negative permittivity meta-material structure in Fig. 17(b). Therefore the negative permittivity meta-material structure is operated as inductance  $L_m$  in equivalent circuit. The negative permittivity meta-material structure is used for impedance matching and high performance of small monopole antenna.

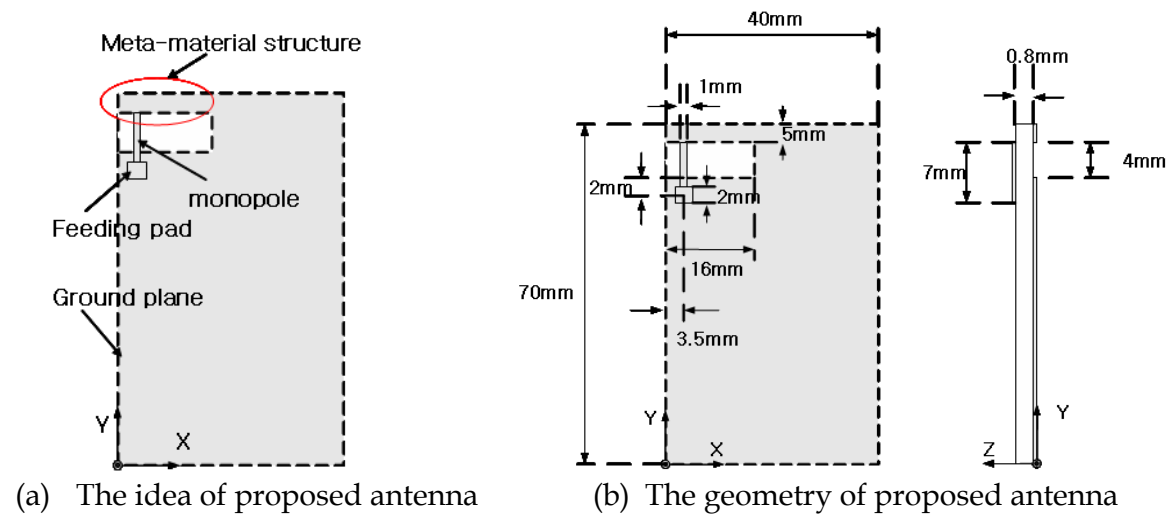


Fig. 15. The concept and geometry of proposed antenna

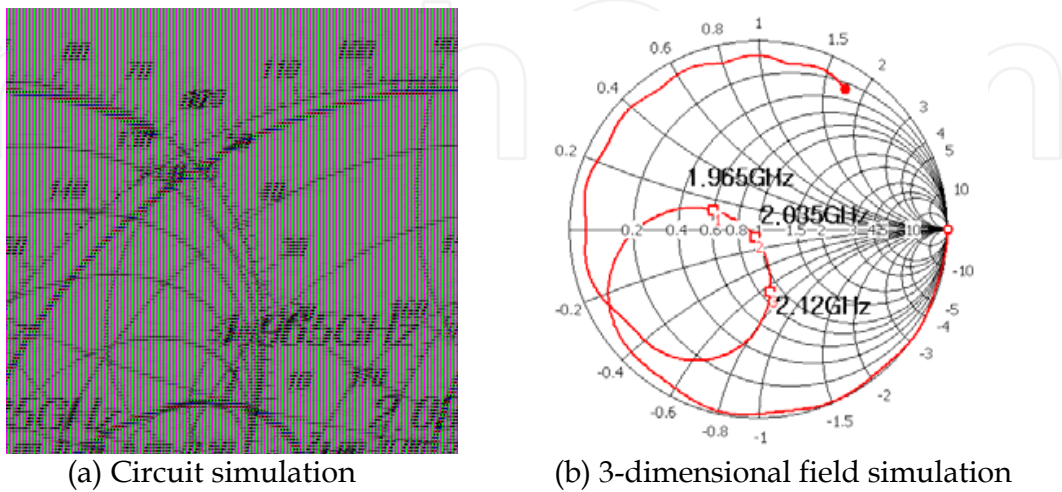


Fig. 16. The loci of input impedance on a smith chart for circuit simulation and 3D field simulation

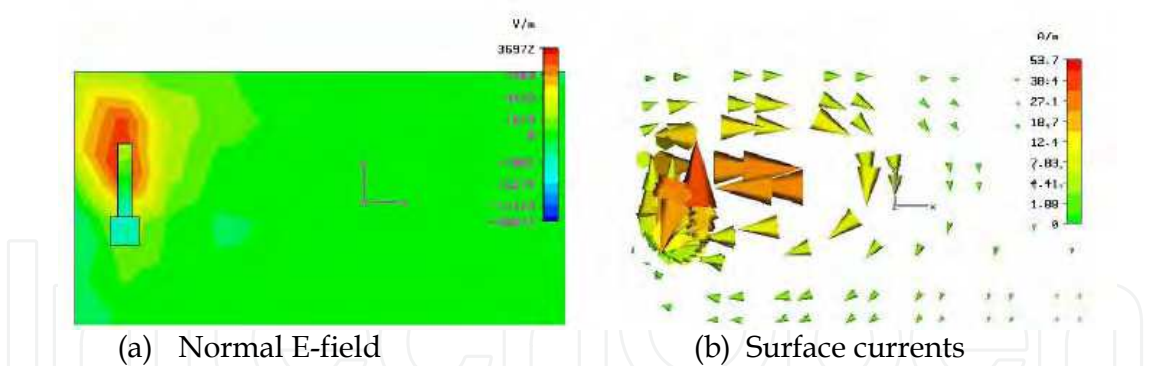


Fig. 17. The field distribution of proposed antenna

The photo of fabricated antenna is shown in Fig. 18(a). The measured return loss is shown in Fig. 18(b). The resonance frequency is 2.04GHz. The measured impedance bandwidth ( $VSRW \leq 2$ ) is 174MHz.

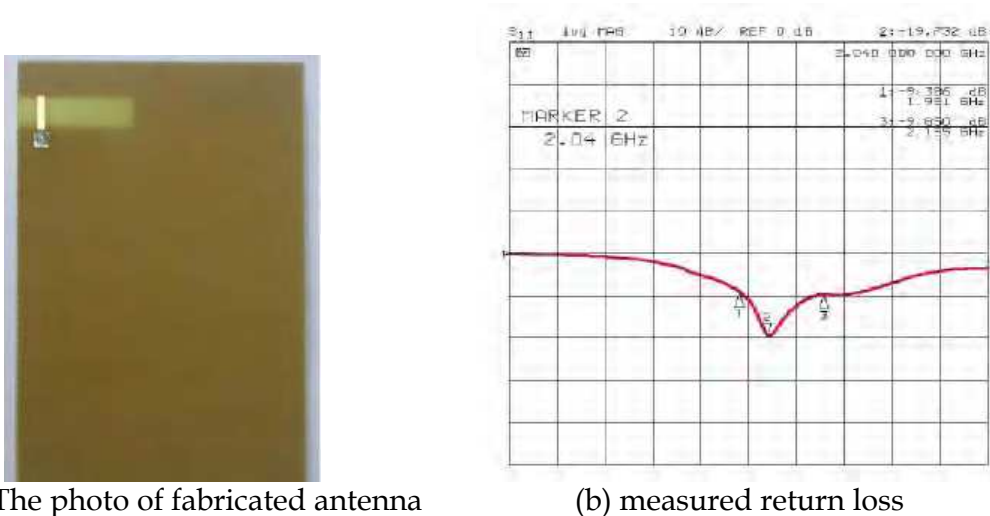


Fig. 18. The photo and measured return loss for proposed antenna

The inner cylinder of coaxial probe and monopole are dominant section of radiation pattern. Therefore, the omni directional pattern is achieved. The values of efficiencies and maximum gains are shown in Table 3. The maximum gain and efficiency are 3.6dBi and 77.8% respectively at the frequency of 2.1GHz. We calculate theoretical quality factor( $Q_L$ ), which is 108, using maximum length of monopole and measured quality factor ( $Q_m$ ), which is 7.21, using fractional bandwidth. We find that the quality factor is lowered by negative permittivity meta-material structure and the improvement of small antenna can be achieved by meta-material concepts.

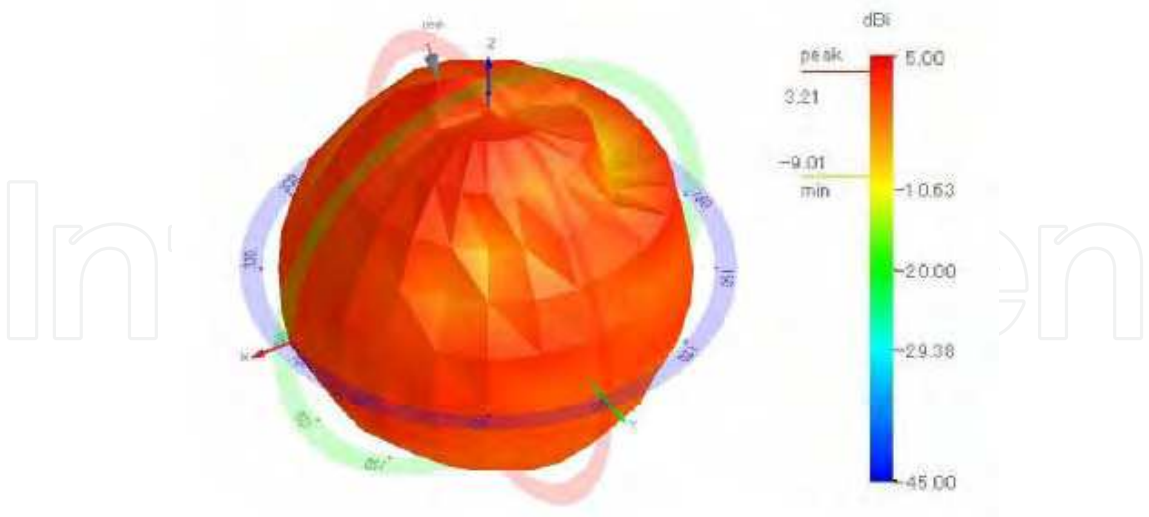


Fig. 19. The measured radiation pattern of fabricated antenna

| Frequency [MHz] | Maximum gain [dBi] | Efficiency |
|-----------------|--------------------|------------|
| 1900            | 2.036              | 49.97%     |
| 2000            | 2.982              | 72.36%     |
| 2040            | 2.986              | 73.64%     |
| 2100            | 3.603              | 77.76%     |
| 2200            | 2.487              | 64.89%     |
| 2300            | 2.128              | 53.50%     |

Table 3. The values of efficiencies and maximum gains

5. Directive radiation of electromagnetic wave using dual-band artificial magnetic conductor structure

5.1 Introduction

In this paragraph, the FSS and AMC structures can be analyzed by a view point of effective medium. So we will find means of FSS and AMC using new analysis method, which will be proposed using periodic boundary condition. The verified FSS and AMC structure will be applied to enhance directivity of antenna. The enhancement of directivity of antenna will be achieved by febyry perot resonance condition between FSS and AMC structure.

5.2 The enhancement of directivity using FSS structure

The meta-materials concept can be realized by electrical structures, which adjust refractive index of material. So we can achieve enhancement of directivity using FSS structure, which is analyzed in negative permittivity of effective medium.

The febyry perot interferometer is shown in Fig. 20. The source generates wave power ( $P_i \cos \theta$ ), which propagates to medium 2 and is reflected. The reflected wave power is



propagated to medium 1 and reflected by medium 1. The generated and reflected wave powers are combined. The reflected wave power ( $P_r$ ) and total power ( $P_t$ ) of generated and reflected wave are expressed by equation (6) and equation (7) briefly.

$$P_r = P_i \cos \left( 2 \frac{2\pi}{\lambda} \cdot d + \phi_1 + \phi_2 + \theta \right) \quad (6)$$

$$P_t = P_i \cos \theta + P_r \quad (7)$$

Where, the  $d$ ,  $\phi_1$ ,  $\phi_2$  and  $\theta$  are distance, phase variation at medium 1, shifted phase at medium 2 and initial phase respectively. These equations didn't consider radiation loss and additional reflected wave.

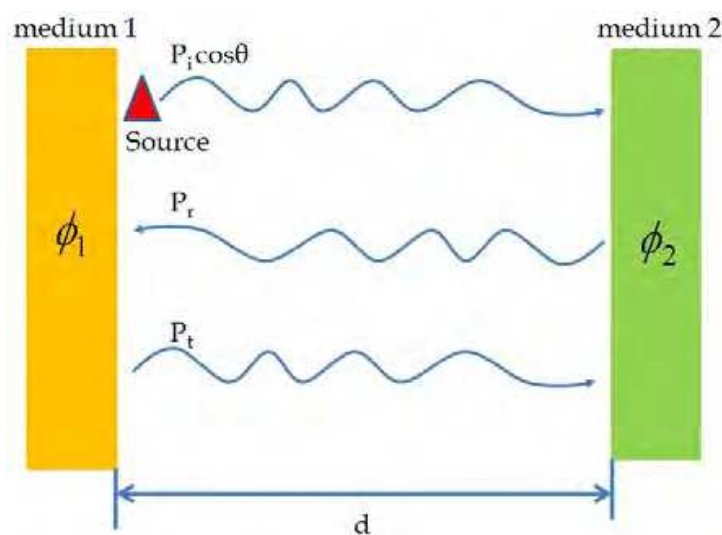


Fig. 20. The febry perot interferometer

If the medium 1 and medium 2 are perfect electric conductor, the shifted phase ( $\phi_1, \phi_2$ ) of medium is 180 degree. Therefore, if the distance is  $\lambda/2$  between medium 1 and medium 2, the total power is maxed.

The enhancement of directivity can be achieved by FSS structure. The source, medium 1 and medium 2 are replaced with antenna, ground and FSS structure. The optimized distance is about  $\lambda/2$  between ground and FSS structure. If the periodic spaces between lattices are very short below one wave length.

The FSS can be analyzed at a point view of effective medium. The equivalent effective permittivity ( $\epsilon_{\text{eff}}$ ) of FSS structure is expressed by equation (8).

$$\epsilon_{\text{eff}} = 1 - \omega_p^2 / \omega^2 \quad (8)$$

Where, the  $\omega_p$  is plasma angular frequency, the  $\omega$  is avaiable angular frequency.

The effective permittivity is negative below plasma angular frequency, however the effective permittivity of FSS structure is near 0 over plasma angular frequency. This characteristic is applicable for enhancement of directivity. The concept of lens using FSS structure is shown in Fig. 21.



But this method has pebry ferot resonance distance, which is  $\lambda/2$ , between FSS strucuture and antenna. The physical height is very large in antenna using FSS structure. If we can adjust shifted phase of ground plane in antenna, we can reduce distance between FSS structure and antenna. So we will find AMC for miniaturization of distance in next paragraph.

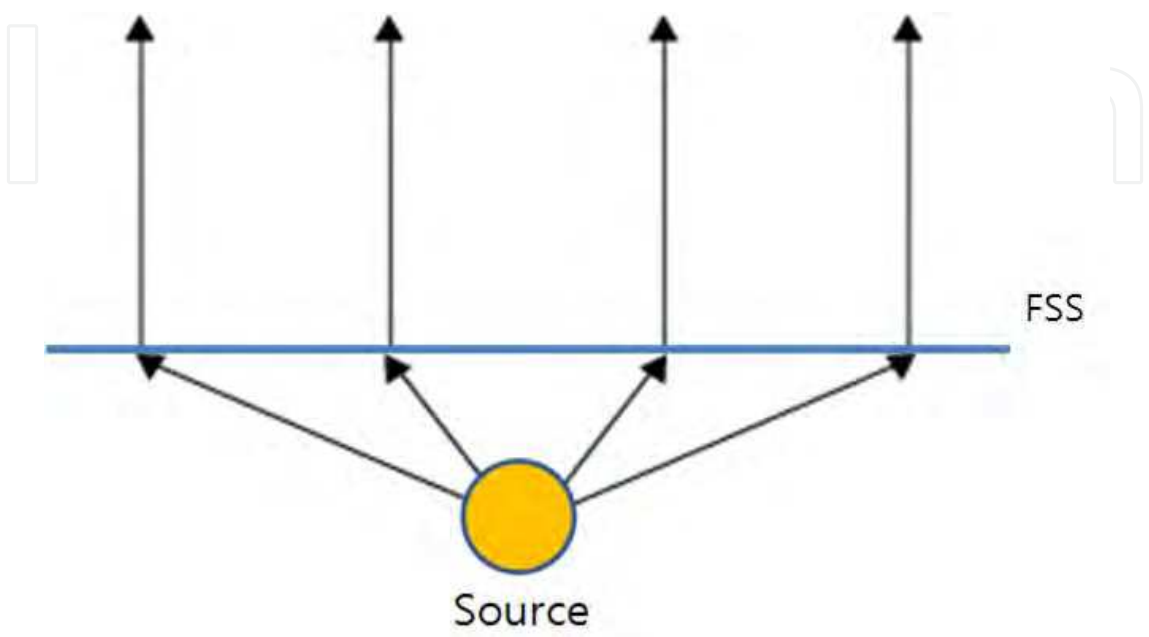


Fig. 21. The concept of lens using FSS strucuture

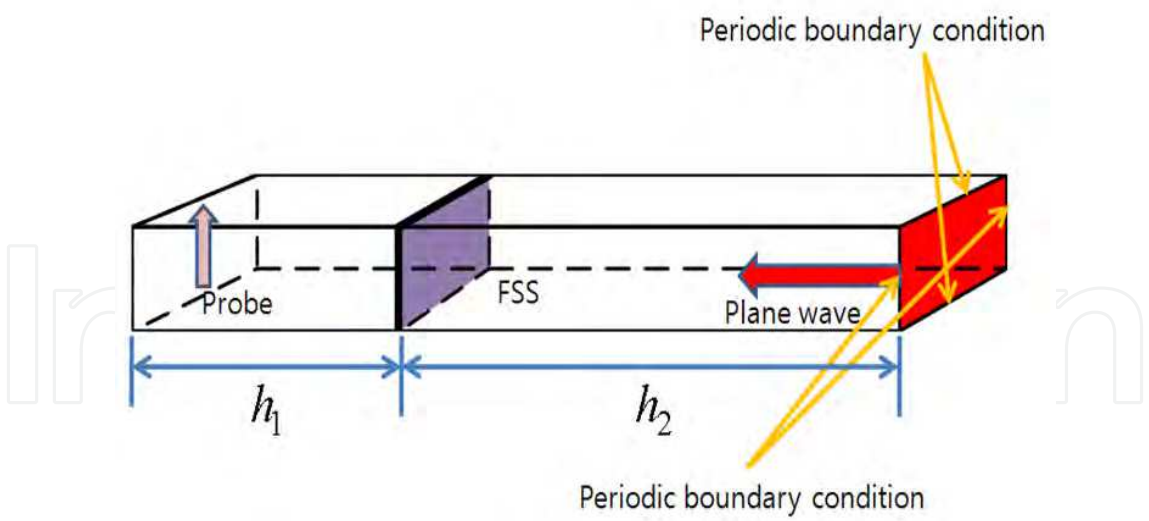


Fig. 22. The analysis method for FSS

**5.3 The enhancement of directivity using FSS structure**

In this paragraph, we propose analysis method for FSS, which is expressed by Fig. 22. The incident plane wave is propagated to unit cell of FSS. The space ( $h_2$ ) between unit cell of FSS and plane wave source is  $\lambda_0$ . The space ( $h_1$ ) between FSS and probe is  $\lambda_0/4$ . These are enclosed by periodic boundary condition.

We think that the plane wave, unit cell of FSS and probe are alternated with signal, FSS plate and receiving antenna. So if the electric filed of received signal is maxed, the unit cell of FSS is operated as FSS lens. The unit cell of FSS structure is shown in Fig. 23. The unit cell is designed using square ring slit on substrate. The substrate is Reogers RO3210, the thickness and relative permittivity are 1.27mm and 10.2 respectively. The unit cell of FSS is alternated with infinite FSS plate using periodic boundary condition.

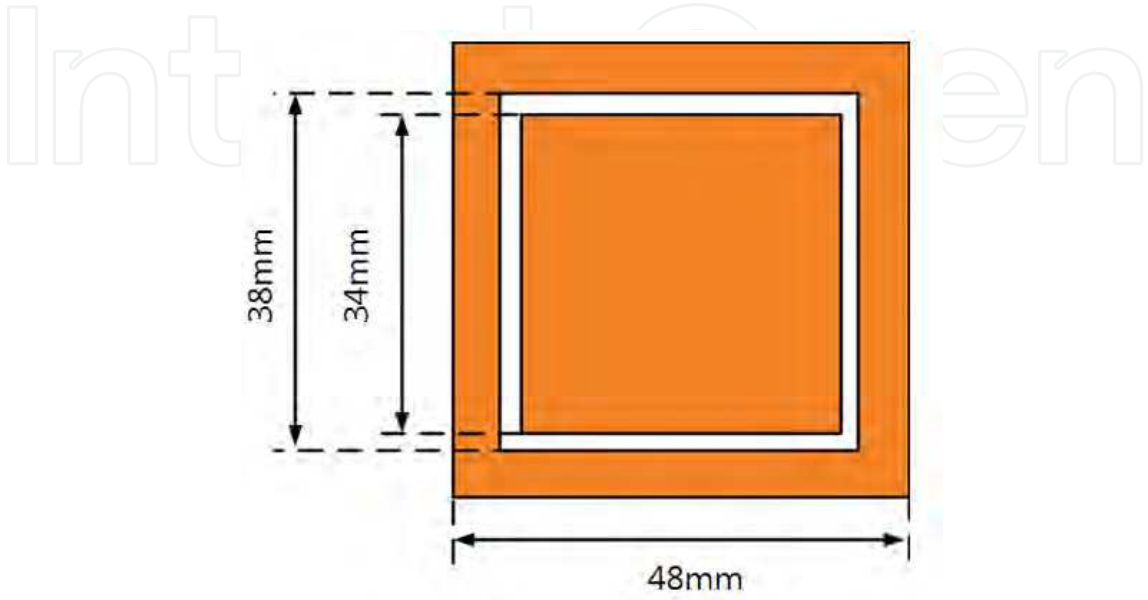


Fig. 23. The unit cell of FSS structure

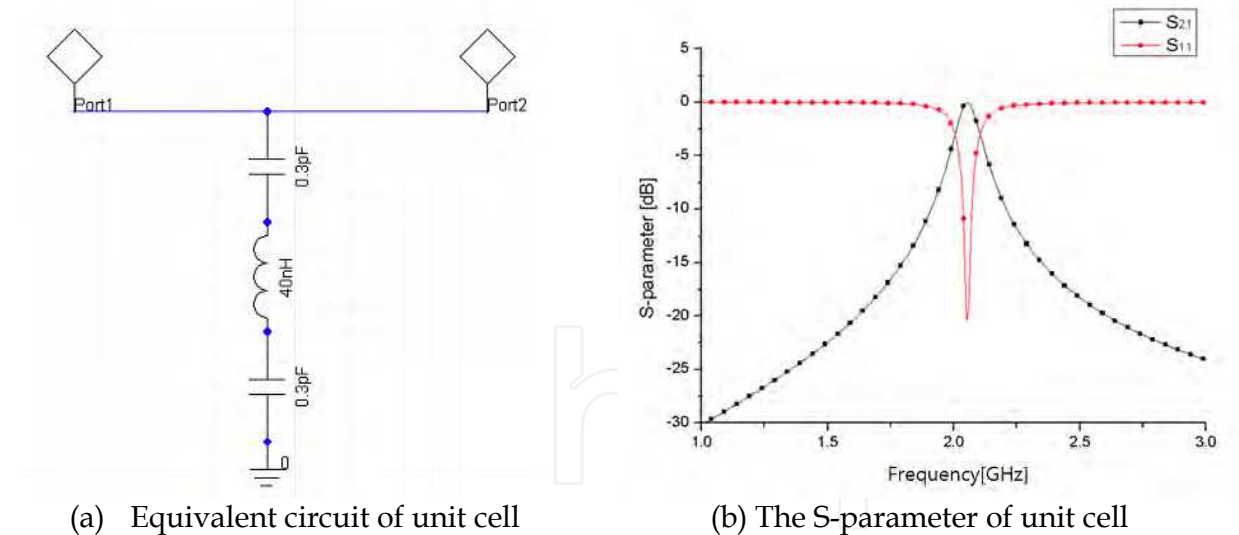


Fig. 24. The unit cell of FSS structure

We think that the infinite conductor plate with periodic square ring slits. If the conductor plate with periodic square ring slits is excited by plan wave, the difference voltage between inner conductor and outer conductor is generated by square slits and the currents are induced along conductor. Therefore, the capacitance is generated between inner conductor and outer conductor.

The inductance is provided by induced currents. The equivalent circuit and S-parameter of unit cell is shown in Fig. 24. The generated capacitance and inductance are 0.3pF and 40nH.

The received E-field is shown in Fig. 25(a). It is maximum E-field at 2GHz. The fractional band width is 950MHz (1.6GHz~2.55GHz). The phase of received signal is expressed in Fig. 25(b). The phase of received signal is 90° at 2GHz.

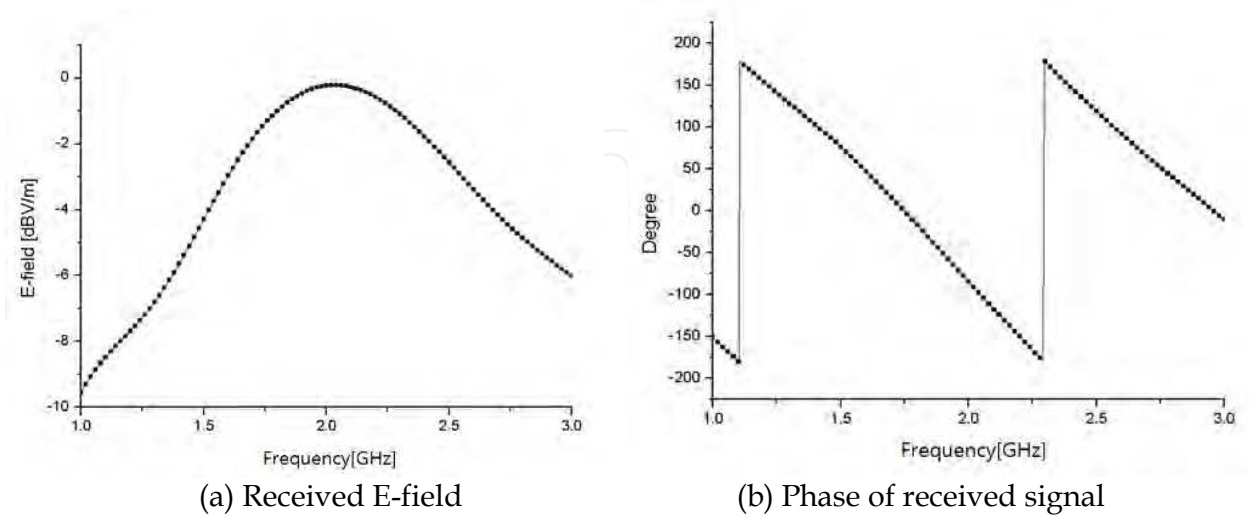


Fig. 25. The unit cell of FSS structure

5.3 The enhancement of directivity using AMC structure

In this paragraph, we find mean of AMC and propose the dual band AMC structure, because the defect of AMC technology is narrow operation bandwidth.

We suppose that the vertical plane wave is propagated to boundary between medium 1 and medium 2. The incident plan wave at boundary between medium 1 and medium 2 is shown in Fig. 26. The Electromagnetic field of incident plane wave can be expressed by equation (9)

$$\vec{E}_1(z) = \vec{a}_x E_{i0} e^{-j\beta_1 z}, \qquad \vec{H}_1(z) = \vec{a}_y \frac{E_{i0}}{\eta_1} e^{-j\beta_1 z} \tag{9}$$

Where, the  $E_{i0}$ ,  $\beta_1$  and  $\eta_1$  are magnitude, phase constant and wave impedance at medium 1. The incident plane wave is divided by discontinuous mediums. A part of incident plane wave is transmitted continuously in medium 2. The rest part is reflected at boundary. The reflected plane wave is expressed by following equation.

$$\vec{E}_r(z) = \vec{a}_x E_{r0} e^{j\beta_1 z}, \qquad \vec{H}_r(z) = -\vec{a}_z \times \frac{1}{\eta_1} \vec{E}_r(z) = -\vec{a}_y \frac{E_{r0}}{\eta_1} e^{j\beta_1 z} \tag{10}$$

The transmitted plane wave is expressed by following equation

$$\vec{E}_t(z) = \vec{a}_x E_{t0} e^{-j\beta_2 z}, \qquad \vec{H}_t(z) = \vec{a}_z \times \frac{1}{\eta_2} \vec{E}_t(z) = \vec{a}_y \frac{E_{t0}}{\eta_2} e^{-j\beta_2 z} \tag{11}$$

Where,  $E_{t0}$ ,  $\beta_2$  and  $\eta_2$  are magnitude, phase constant and wave impedance respectively at  $z=0$ .

The relation of electric fields and magnetic fields can be expressed by equation (12)

$$\vec{E}_i(0) + \vec{E}_r(0) = \vec{E}_t(0), \quad \vec{H}_i(0) + \vec{H}_r(0) = \vec{H}_t(0) \tag{12}$$

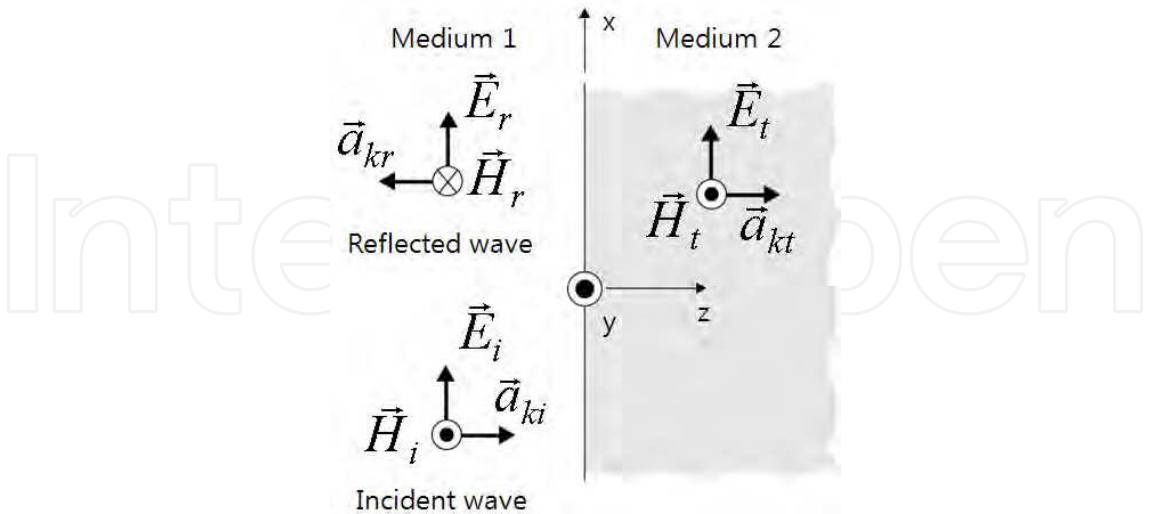


Fig. 26. The incident plan wave at boundary between medium 1 and medium 2

The magnetic field can be replaced with electric field using wave impedance and expressed by equation (13)

$$\frac{1}{\eta_1} (E_{i0} - E_{r0}) = \frac{E_{t0}}{\eta_2} \tag{13}$$

The reflection and transmission electric fields are expressed by equation (14) using equation (12) and (13).

$$E_{r0} = \frac{\eta_2 - \eta_1}{\eta_2 + \eta_1} E_{i0}, \quad E_{t0} = \frac{2\eta_2}{\eta_2 + \eta_1} E_{i0} \tag{14}$$

The reflection and transmission coefficient can be extracted using equation (14). The reflection and transmission coefficients are following equation (15).

$$\Gamma = \frac{E_{r0}}{E_{i0}} = \frac{\eta_2 - \eta_1}{\eta_2 + \eta_1}, \quad \tau = \frac{E_{t0}}{E_{i0}} = \frac{2\eta_2}{\eta_2 + \eta_1} \tag{15}$$

We see the reflection coefficient. If medium 2 is conductor, the wave impedance ( $\eta_2$ ) is 0. So reflection coefficient is -1. But if medium 2 has very high impedance like as infinity impedance, the reflection coefficient is 1. Therefore, the mean of AMC is electrical structure for infinity wave impedance. The wave impedance ( $\eta_2$ ) is following equation (16)

$$\eta_2 = \sqrt{\frac{\mu_2}{\epsilon_2}} \tag{16}$$

Finally, the AMC can be achieved by near zero permittivity or infinity high permeability. How can we achieve AMC structure? The realization of AMC can be found using resonance structure. The representative AMC structure, which is mushroom structure and equivalent circuit are shown in Fig 27.

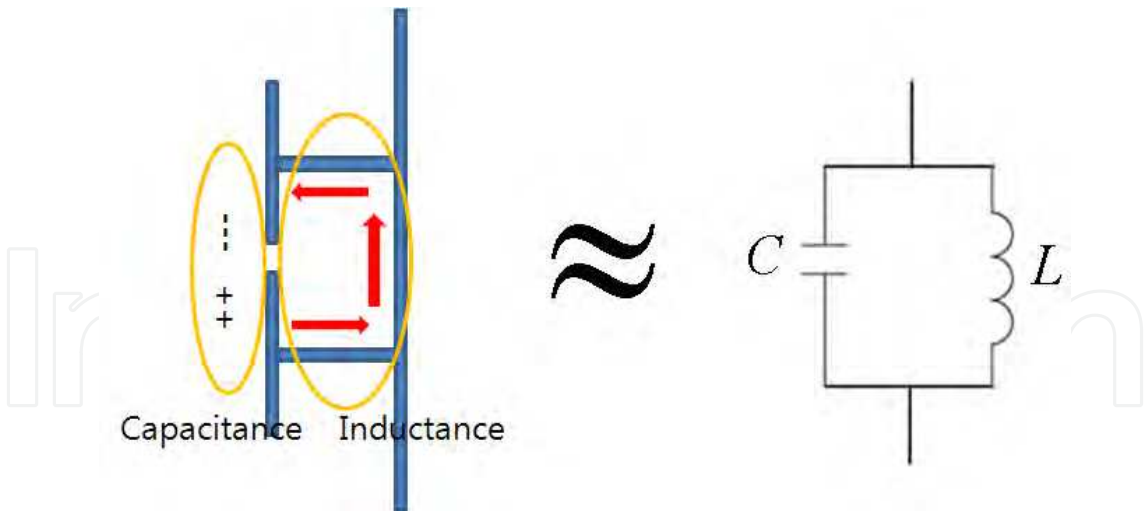


Fig. 27. The mushroom structure and equivalent circuit

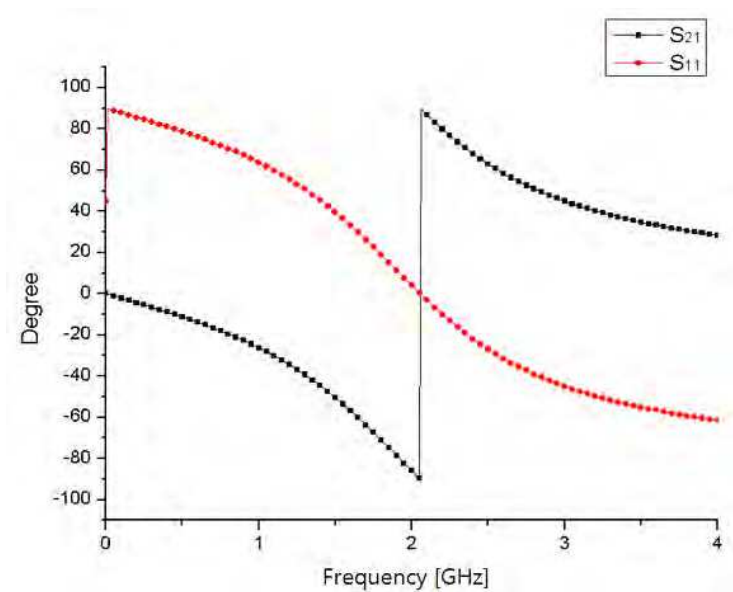


Fig. 28. The reflection coefficient phase and transmission coefficient phase

We find that the mushroom structure is like as split ring resonator. The mushroom structure is operated as parallel resonator. The capacitance is generated between plates of periodic mushroom structures. The inductance is induced by surface currents.

If the capacitance ( $C$ ) and inductance ( $L$ ) are 1pF and 6nH, the resonance frequency is 2.05GHz. The reflection coefficient phase and transmission coefficient phase are shown in Fig. 28. We analyze phase of transmission coefficient based on point view of effective medium. The negative phase is inductance section, which is alternated with negative epsilon medium or high permeability medium below 2.05GHz. otherwise the positive phase is expressed by high permittivity or negative permeability.

If the operating frequency is near 2.05GHz, the mushroom structure achieves high impedance structure. The proposed analysis method of AMC is shown in Fig. 29. The reflection coefficient is very important in AMC structure. The probe is set at location of plan

wave port. If the distance is — between unit cell of AMC and plan wave port, the received electric field is maximum strength, which is detected by probe. Because the reflected wave phase and excited phase has same phase. If the AMC is replaced with perfect electric conductor, the received electric filed is very small strength.

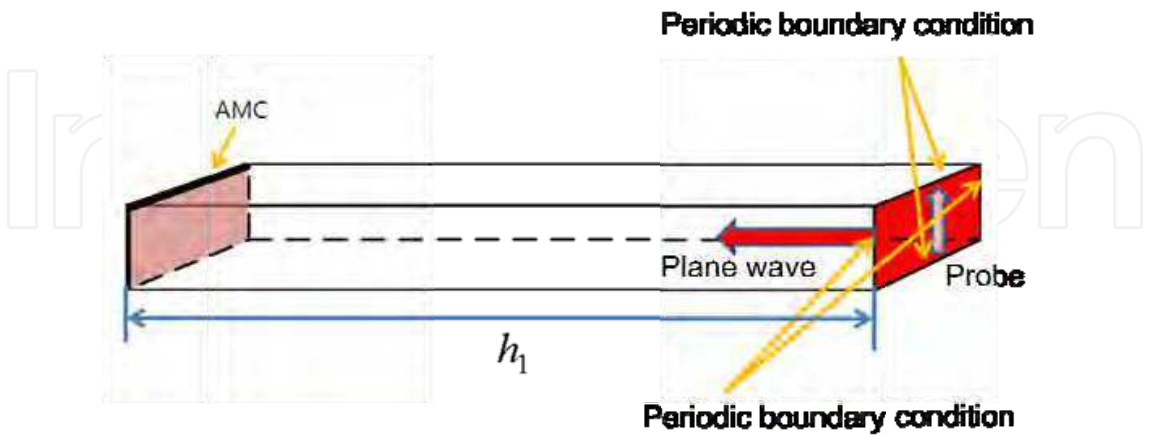


Fig. 29. The proposed analysis method of AMC

We try to design of dual band AMC using proposed method. The proposed unit cell of dual-band AMC structure is shown in Fig. 30. The substrates are RO3210 of Rogers , thickness is 1.27mm. We see tho middle layer. The vias are added for miniaturization of proposed AMC. The parallel short circuit structures, are used for wide AMC operation bandwidth, are realized by slits. The dual AMC operation frequency is realized using stacked thin lines above middle layer. The proposed unit cell of dual band AMC structure is analyzed by proposed analysis method of AMC. The received electric field strength of dual-band AMC is shown in Fig. 31. The operation bandwidth (E-field>0dB) are 120 MHz (1.85GHz~1.98GHz) and 70 MHz (2.11GH ~2.18GHz) respectively.

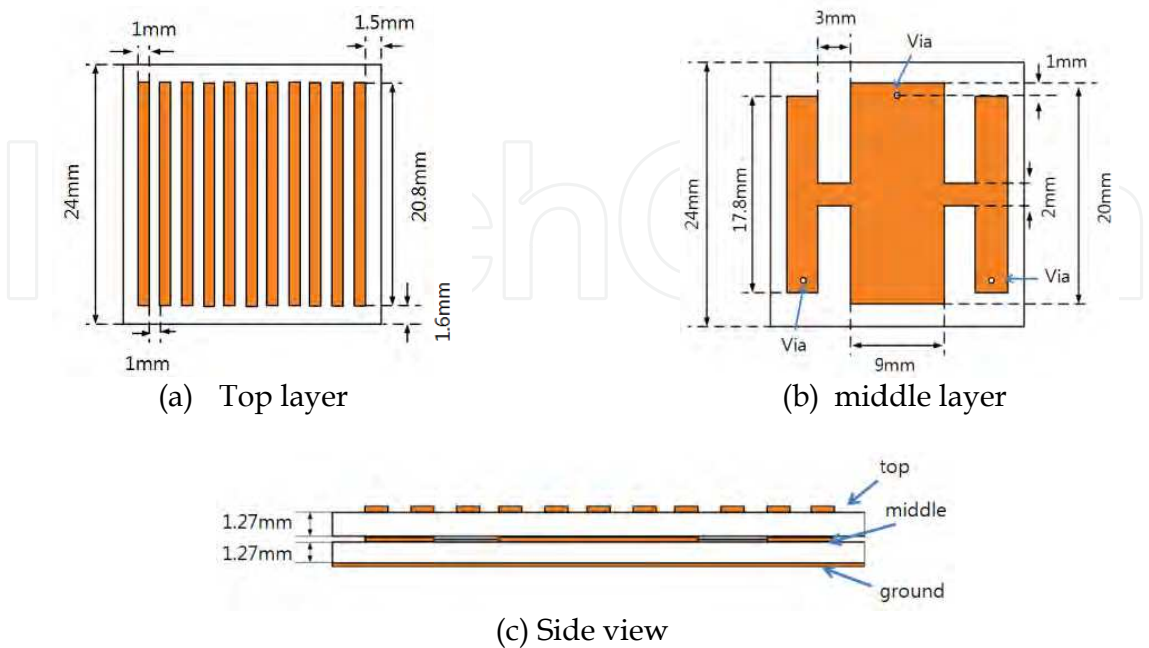


Fig. 30. The proposed dual-band AMC structure



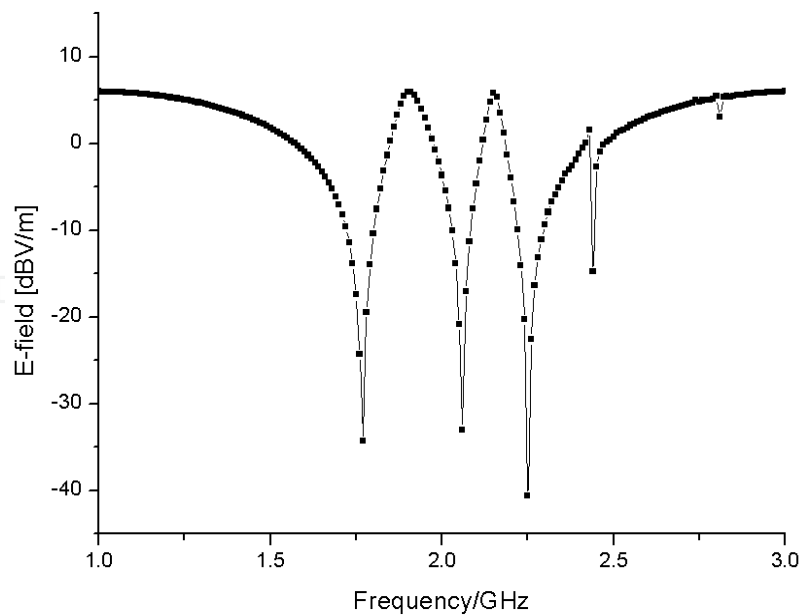


Fig. 31. The proposed dual-band AMC structure

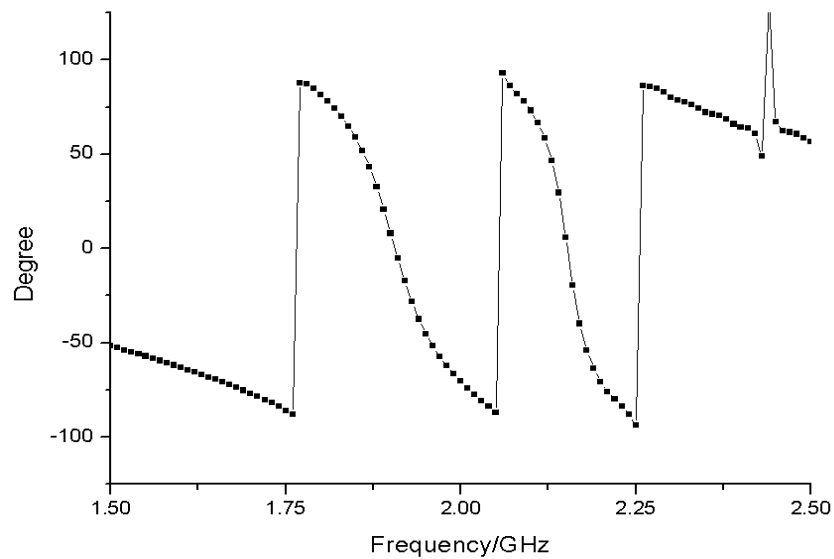


Fig. 32. The phase of proposed dual-band AMC structure

The phase response of dual band AMC is shown in Fig. 32. There are maximum received signal strengths and 0 phases at 1.91GHz and 2.15GHz respectively. Therefore, we find that proposed dual-band AMC is operated as AMC plane at 1.91GHz and 2.15GHz. The antenna gain can be improved by FSS, but this method has defect of long height, which is febrly perot resonance condition ( $\frac{\lambda_0}{2}$ ) between FSS and antenna ground. However, if the antenna ground is replaced with dual-band AMC structure, the distance between antenna ground and FSS is reduced and compact size. It is the composition structure of AMC and FSS analysis to spend very long time, because composition structure is analyzed fully in 3-D filed simulation, so we propose convenient analysis method for composition structure. We estimate composition of proposed unit cell

of FSS structure and dual-band AMC structure using proposed analysis method. The proposed analysis method for composition of AMC and FSS is shown Fig. 33.

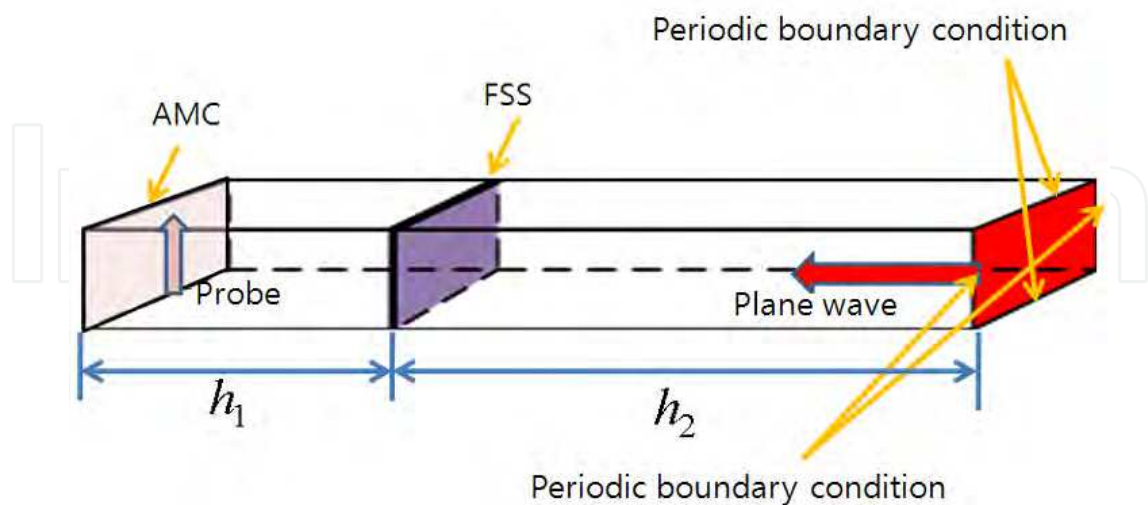


Fig. 33. The proposed analysis method for composition AMC and FSS

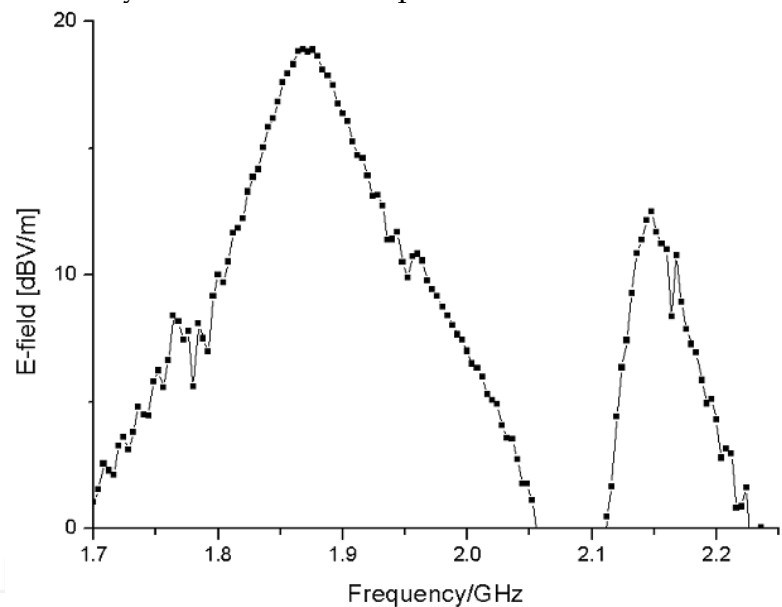


Fig. 34. The proposed analysis method for composition AMC and FSS

The proposed analysis method is very fast and convenient for optimization of distance between AMC and FSS. The distance( $h_1$ ) between AMC and FSS is about  $\lambda_0/4$ . The distance ( $h_2$ ) between plane wave source and FSS is  $\lambda_0$ . The probe is set on AMC plane. If the probe is regarded as antenna, the received electric field is max at operation frequency. The received electric field strength for proposed composition of FSS and AMC is shown in Fig. 34. The received electric field strengths are max at AMC operation frequencies, which are 1.87GHz and 2.15GHz.

The proposed composition structure will be applied to microstrip patch antennas. The proposed microstrip patch antenna using dual-band AMC is shown in Fig. 35. The proposed microstrip patch antennas are designed for 1.9GHz and 2.1GHz respectively. The 1.9GHz and 2.1GHz micrpstrip patch antenna size (p) are 23 mm and 20.4mm respectively. The

feeding positions (d) are 2.1mm and 2.4mm respectively against 1.9GHz and 2.1GHz microstrip patch antenna.

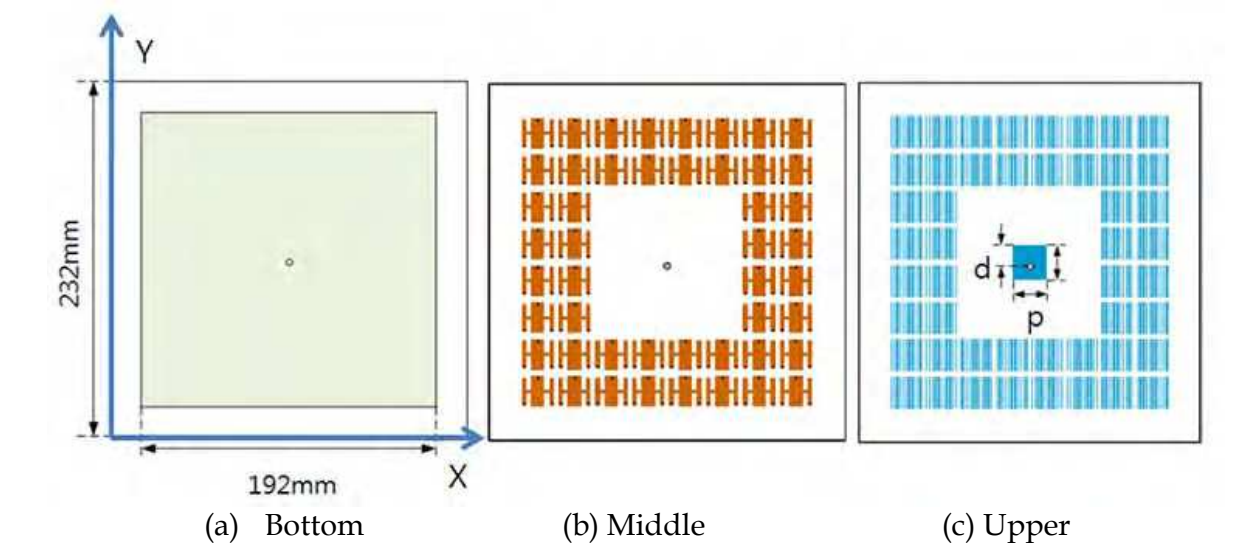


Fig. 35. The proposed microstrip patch antenna using dual-band AMC

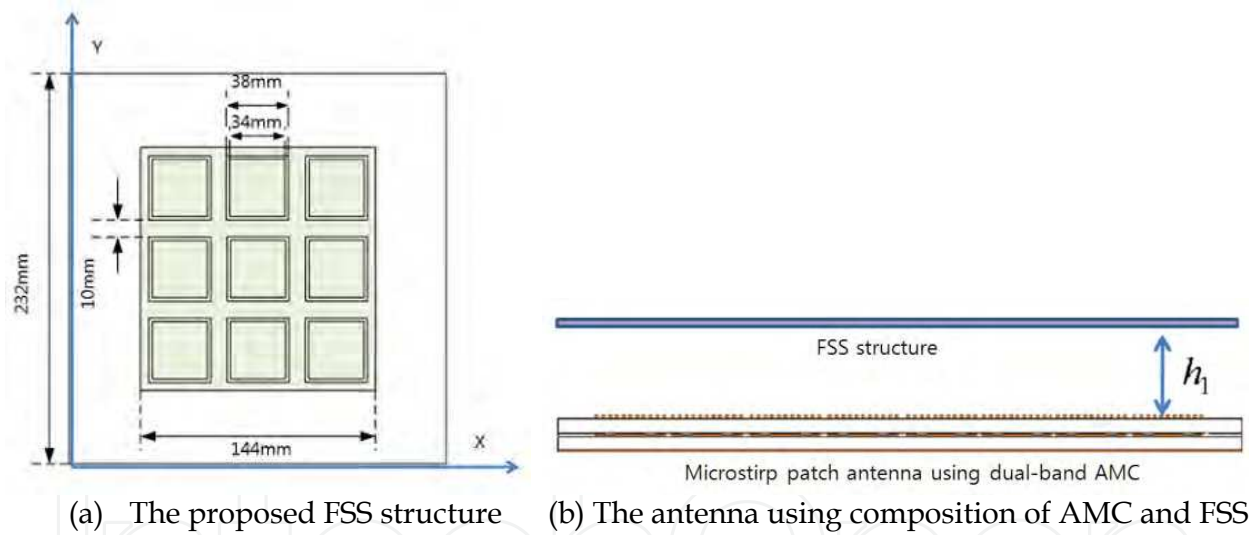


Fig. 36. The proposed FSS structure and the antenna using composition of AMC and FSS

The proposed FSS structure and the antenna using composition of AMC and FSS are shown in Fig. 36. The height ( $h_1$ ) between FSS structure and dul-band AMC is 10mm, which is very short length. The reduction of height can be adjusted using reflection phase of AMC structure. The photos of fabricated antennas are shown in Fig. 37. The total size of the antenna using composition is  $232\text{mm} \times 232\text{mm} \times 13.81\text{mm}$ . The substrates of FSS and antenna are RO3210( $\epsilon_r$ : 10.2) of Rogers.

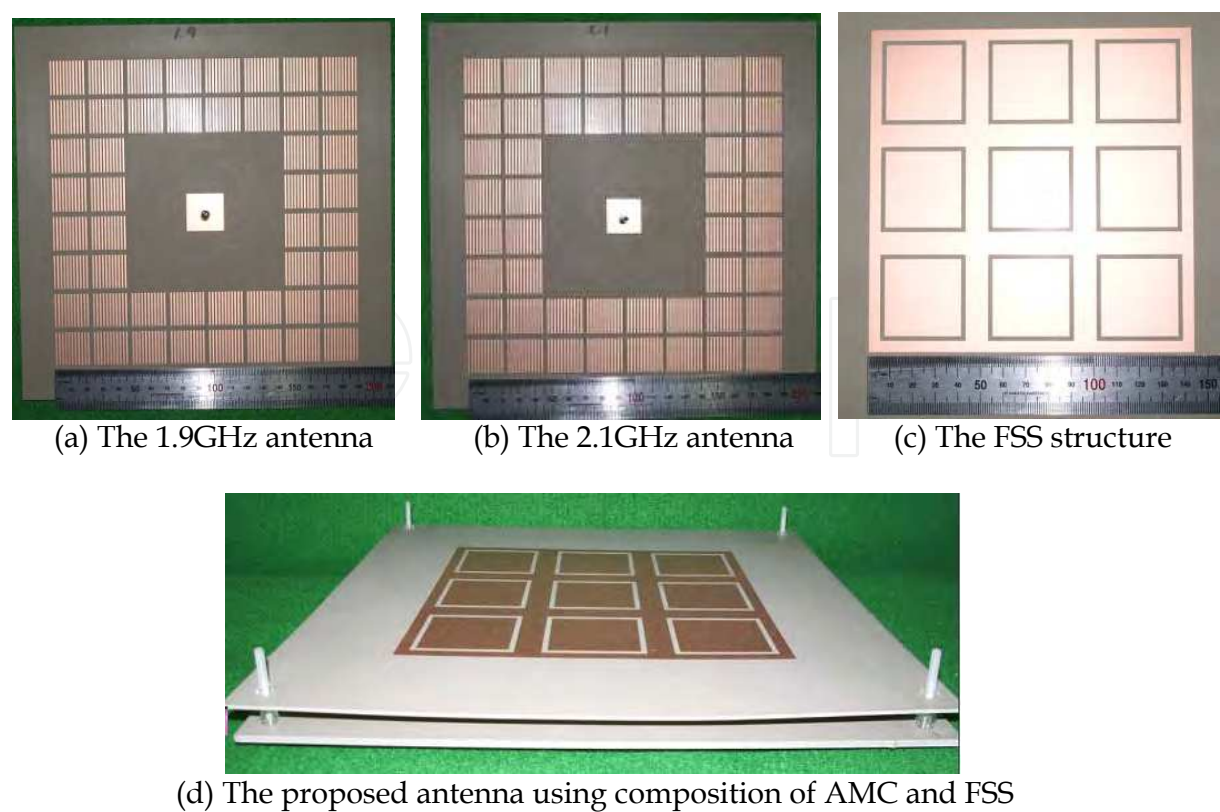


Fig. 37. The photos of fabricated antennas

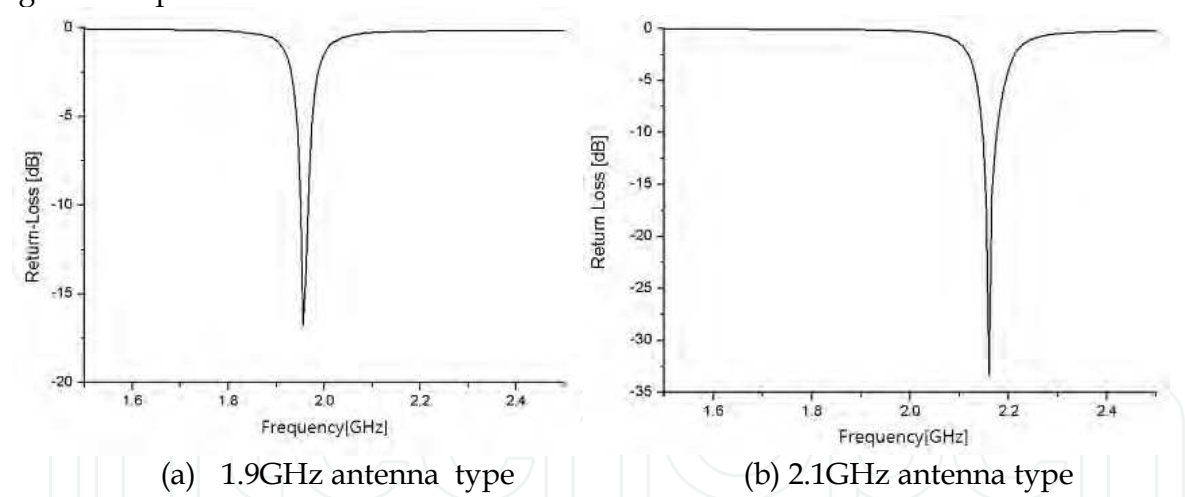


Fig. 38. The measured return-loss against antenna types

The measured return-losses against antenna types are shown in Fig. 38. The resonance frequency and impedance bandwidth ( $VSWR \leq 2$ ) are 1.97GHz and 20MHz respectively in the 1.9GHz antenna type. The resonance frequency and impedance bandwidth ( $VSWR \leq 2$ ) of 2.1GHz antenna type are 2.17GHz and 20MHz. The radiation patterns against antenna types are shown in Fig. 39. We measure antenna against three states. One state is conductor ground type, another state is AMC ground type. The other state is composition of AMC ground and FSS structure. The antenna gain and FBR (front back ratio) of 1.9GHz and 2.1GHz antennas are shown in table 4. We find that the back lobe of 1.9GHz antenna is reduced by AMC structure, because the surface wave is suppressed by AMC. The

maximum gain of composition type is 9.1 dBi although low profile, which is 10mm, between AMC and FSS. But the surface wave suppression is not good at 2.1GHz antenna type. The aspect of measured data is very similar to the estimation result for composition AMC and FSS. The maximum gain of 2.1GHz antenna is 9.1dBi.

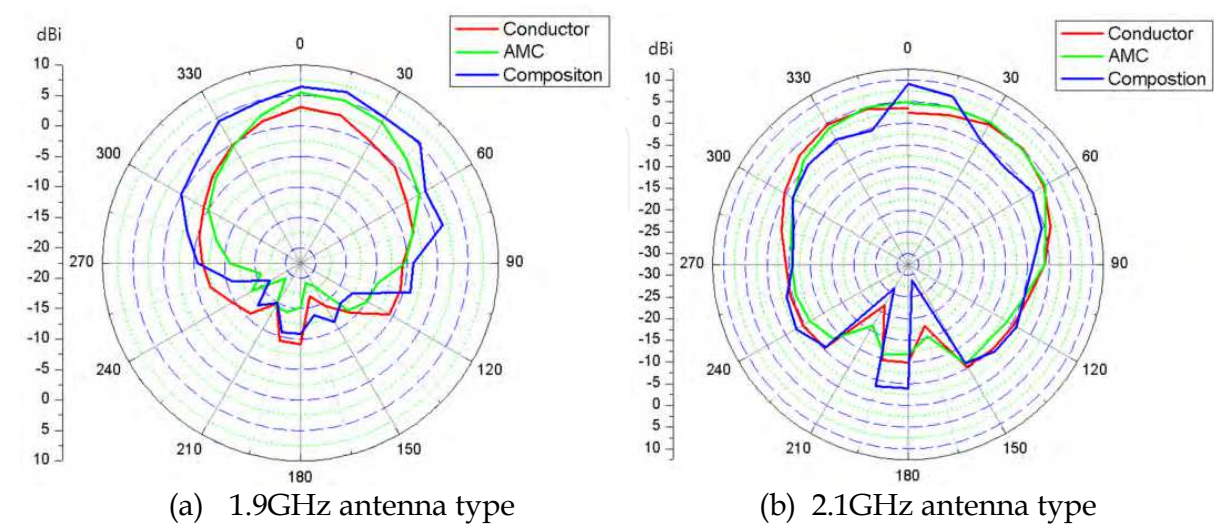


Fig. 39. The measured radiation patterns against antenna types

| Types          |            | Conductor | AMC  | Composition |
|----------------|------------|-----------|------|-------------|
| Characteristic | Gain [dBi] | 4.6       | 7    | 8           |
|                | FBR [dB]   | 13.7      | 22.2 | 18.8        |
| 2.1GHz antenna | Gain [dBi] | 4.6       | 6.5  | 9.1         |
|                | FBR [dB]   | 13.7      | 17.6 | 13          |

Table 4. The antenna gain and FBR against antenna types

The proposed antenna using composition FSS and dual-band AMC structure achieves low profile and high gain. We find that characteristic of the AMC and FSS structure is replaced with material point view.

The AMC is operated like as high permeability. The FSS has near 0 permittivity at operating frequency. Therefore, we can adjust material characteristic by additional electric structures like as meta-material structure.

6. EM waves shielding functional concrete

6.1 Introduction

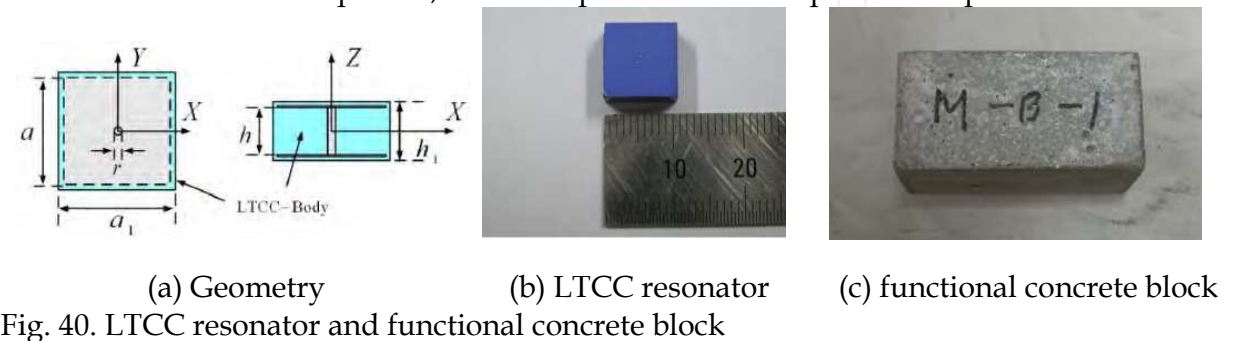
In this pragraph, we try to realize SNG meta-material using LTCC (low temperature cofired ceramic) resonator. The mushroom structure, which is resonator, is designed on ground and reduces surface wave. If the suface wave is replaced with plane wave, the image theory is not applicable in space. Therefore, the mushroom structure must be extended for stop-band characteristic. So we propose LTCC resonator, which is put into concrete for SNG concrete



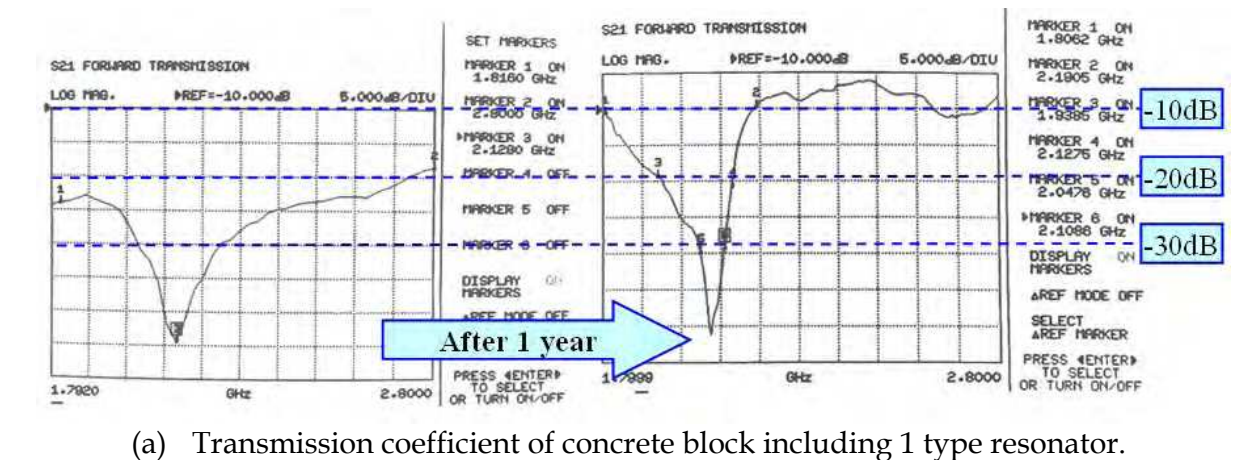
block. we compare the results measured 1 year ago with the recent results. Because concrete block, loss is too high,includes water until it is dried perfectly.

6.2 The EM shielding concreted block using LTCC resonator

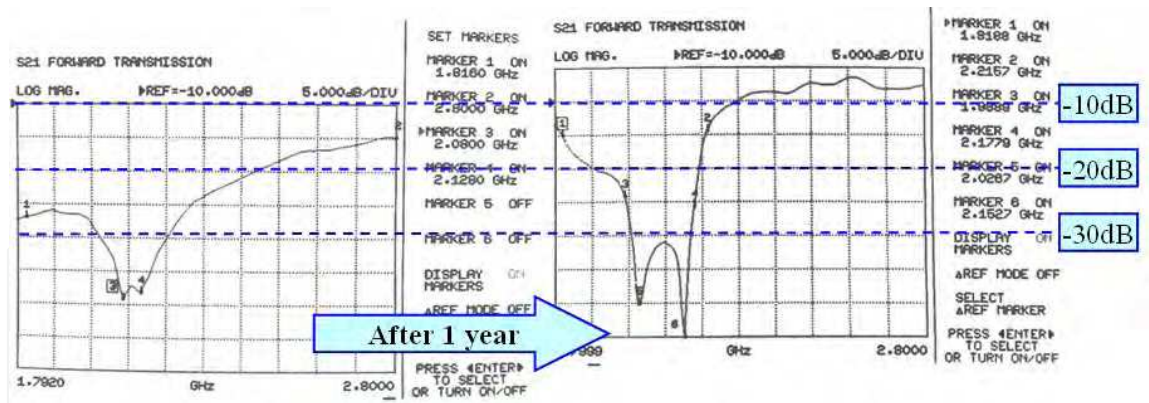
The geometry of unit cell LTCC resonator and photos of resonator and concrete block are shown in Fig. 40. The proposed resonator consists of two square plates and one via in LTCC( $\epsilon_r = 7.8$ ) body. The plate size is 10mm ( $a$ ) $\times$ 10mm( $a$ ). The via length ( $h$ ) is 5mm. LTCC body size is 10.2mm ( $a_1$ ) $\times$  10.2mm ( $a_1$ )  $\times$ 5.2mm ( $h_1$ ). The concrete block size is 80mm $\times$ 40mm $\times$ 40mm. The proposed structure is operated as parallel LC resonator which has a characteristic of stop band, and it is operated like an equivalent dipole.



The proposed structure is operated as parallel LC resonator which has a characteristic of stop band, and it is operated like an equivalent dipole. The coefficient comparison of a block with three resonators at 60 days and 1 year are shown in Fig. 41. The transmission coefficient variation of concrete block including only 1 type resonator is shown in Fig. 41 (a). As concrete loss level is lowered from -15dB (60 days) to -5dB (1 year), bandwidth of stop band is changed according to time. The transmission coefficient variation of concrete block including 2 kinds of resonator is shown in Fig. 41 (b). All these results show that the change in the dielectric properties strongly related to the amount of water in the concrete block and the permittivity changes may vary the stop band width and resonance frequency.





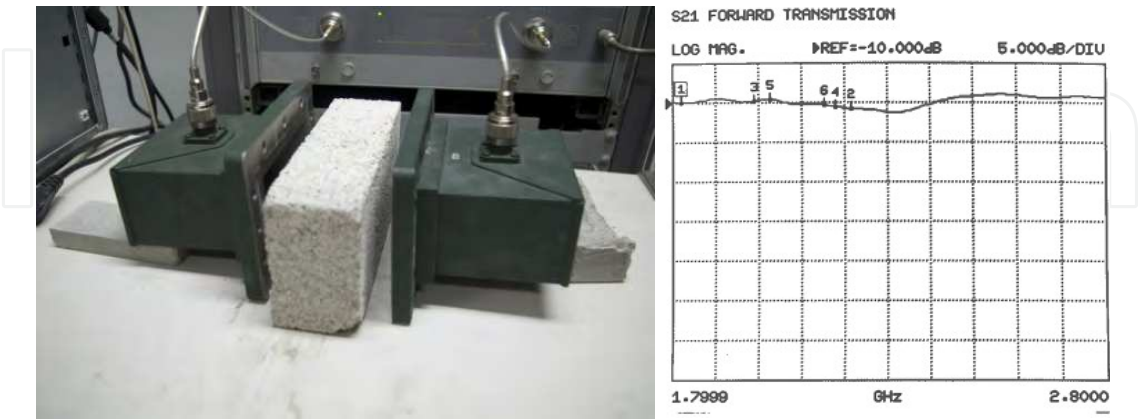


(b) Transmission coefficient of concrete block including 2 kinds of resonators  
Fig. 41. The coefficient comparison of a block with three resonators at 60 days and 1 year

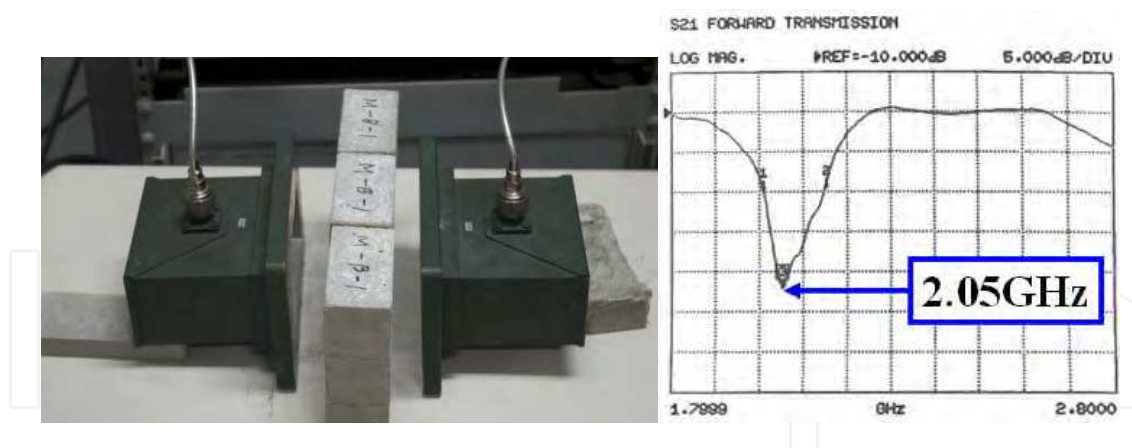
| Block type | Mixer ratio | Resonance Frequency (GHz) |              | Bandwidth (MHz)         |        |                         |        |                         |        |
|------------|-------------|---------------------------|--------------|-------------------------|--------|-------------------------|--------|-------------------------|--------|
|            |             |                           |              | ( $\leq -10\text{dB}$ ) |        | ( $\leq -20\text{dB}$ ) |        | ( $\leq -30\text{dB}$ ) |        |
|            |             | 60 days                   | 1 year       | 60 days                 | 1 year | 60 days                 | 1 year | 60 days                 | 1 year |
| M-B-1      | 73.42:1     | 2.12                      | 2.07         | -                       | 395    | -                       | 191    | 215                     | 90     |
| M-AB-2     | 36.21:1     | 2.08<br>2.12              | 2.02<br>2.15 | -                       | 550    | -                       | 294    | 175                     | 167    |

Table 5. The characteristic of functional concrete block against time

In order to apply the real building environment, concrete wall models are simulated. The pure concrete wall model is a single concrete block without resonator, and concrete wall model consists of 6 concrete blocks including resonator. The photos and transmission coefficients of concrete walls with/without LTCC resonators are shown in Fig. 42. We find that the functional concrete block achieve SNG material characteristic using LTCC resonator and is applicable for shielding structure.



(a) Concrete block without resonator



(b) Concrete block with LTCC resonators

Fig. 42. The photos and transmission coefficients of concrete walls with/without LTCC resonators

## 7. Conclusion

In this chapter, we study means of meta-material concept using transmission line, the NPLH transmission line, the compact antenna using meta-material concepts, the directive radiation of electromagnetic wave using dual-band artificial magnetic conductor structure and EM waves shielding functional concrete. It is proposed electrical structure to change characteristic of material at material point view. If we approach material point view of electrical structure, the component design method and analysis can be extended and will be improved by meta-material concepts

## 8. References

- J. B. Pendry, A. J. Holden, D. J. Robbins, and W. J. Stewart (1998). Low frequency plasmons in thin-wire structures, *Journal of Physics Condensed Matter*, vol. 10, pp. 4785-4810,
- J. B. Pendry, A. J. Holden, D. J. Robbins, and W. J. Stewart (1999). Magnetism from conductors and enhanced nonlinear phenomena, *Microwave Theory and Techniques*, IEEE Trans., vol. 47, pp. 2075-2084
- C. Caloz, H. Okabe, T. Iwai, and T. Itoh (2002). Anisotropic PBG surface and its transmission line model, *URSI Dig., IEEE-AP-S USNC/URSI National Radio Science Meet.*, pp. 224, San Antonio, TX, USA,
- A. Lai, T. Itoh, and C. Caloz (2004). Composite right/left-handed transmission line metamaterials, *Microwave Magazine, IEEE*, vol. 5, pp. 34-50
- A. Sanada, C. Caloz, and T. Itoh (2004). Characteristics of the composite right/left-handed transmission lines, *Microwave and Wireless Components Lett., IEEE*, vol. 14, pp. 68-70
- R. W. Ziolkowski and A. Erentok (2006). Metamaterial-based efficient electrically small antennas, *Antennas Propagat., IEEE Trans.*, vol. 54, pp. 2113-2130
- A. Erentok and R. W. Ziolkowski (2006). An efficient metamaterial-inspired electrically-small antenna, *Microwave Optical Technology Lett.*, vol. 49, pp. 1669-1672

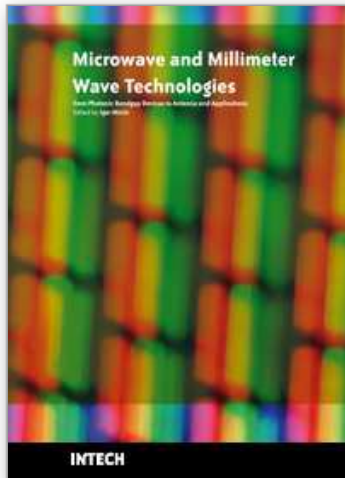
- M. Thevenot, C. Cheype, A. Reineix, B. Jecko, F. des Sci, and L. Cnrs (1999). Directive photonic-bandgap antennas, *Microwave Theory and Techniques, IEEE Trans.*, vol. 47, pp. 2115-2122
- R. Biswas, E. Ozbay, B. Temelkuran, M. Bayindir, M. M. Sigalas, and K. M. Ho (2001). Exceptionally directional sources with photonic-bandgap crystals, *Journal of the Optical Society of America B*, vol. 18, pp. 1684-1689
- S. Enoch, G. Tayeb, P. Sabouroux, N. Gurin, and P. Vincent (2002). A Metamaterial for Directive Emission, *Physical Review Lett.*, vol. 89, pp. 2139-2142
- D. Sievenpiper, L. Zhang, R. F. J. Broas, N. G. Alexopolous, and E. Yablonovitch (1999). High-impedance electromagnetic surfaces with a forbidden frequencyband, *Microwave Theory and Techniques, IEEE Trans.*, vol. 47, pp. 2059-2074
- Feresidis, A.P., and Vardaxoglou, J.C. (2001). High gain planar antenna using optimised partially reflective surfaces, *Microwave Antennas Propag.*, IEE Proc., vol. 148, pp. 345-350
- N. C. Karmakar, M. N. Mollah, and S. K. Padhi (2002). Improved performance of a non-uniform ring patterned PBG assisted microstrip line, *Antennas and Propag. Society International Symposium, IEEE*, vol. 2, pp. 848-851
- E. Brown, C. Parker, E. Yablonovitch (1993). Radiation properties of a planar antenna on a photonic-crystal substrate, *Journal-Optical Society of America B*, vol. 10, pp. 404
- S. Cheng, R. Biswas, E. Ozbay, S. McCalmont, G. Tuttle, K.-M. Ho (1995). Optimized dipole antennas on photonic band gap crystals, *Applied Physics Lett.* vol. 67, pp. 3399
- E. Brown, O. McMahon (1996). High zenithal directivity from a dipole antenna on a photonic crystal, *Applied Physics Lett.*, vol. 68, pp. 1300
- M. Kesler, J. Maloney, B. Shirley, G. Smith (1996). Antenna design with the use of photonic band-gap materials as all-dielectric planar reflectors, *Microwave and Optical Technology Lett.*, vol. 11, pp. 169
- M. Sigalas, R. Biswas, Q. Li, D. Crouch, W. Leung, R. Jacobs-Woodbury, B. Lough, S. Nielsen, S. McCalmont, G. Tuttle, K.-M. Ho (1997). Dipole antennas on photonicband-gap crystals: Experiment and simulation, *Microwave and Optical Technology Lett.*, vol. 15, pp. 153
- C. Caloz and T. Itoh (2006). Electromagnetic Metamaterials: Transmission Line Theory and Microwave Applications: the Engineering Approach, *Wiley-IEEE Press*
- J. B. Pendry and D. R. Smith (2004). Reversing Light With Negative Refraction, *Physics Today*, pp. 37-44
- C. Caloz, H. Okabe, T. Iwai, and T. Itoh (2002). Transmission line approach of left-handed (LH) materials, *Proc. USNC/URSI National Radio Science Meeting*, vol. 1, pp. 39
- S. B. Cohn (2004). Electrolytic-Tank Measurements for Microwave Metallic Delay-Lens Media, *Journal of Applied Physics*, vol. 21, pp. 674
- S. Clavijo, R. E. Diaz, and W. E. McKinzie Iii (2003). Design methodology for Sievenpiper high-impedance surfaces: an artificial magnetic conductor for positive gain electrically small antennas, *Antennas and Propagation, IEEE Trans.*, vol. 51, pp. 2678-2690
- S. K. Hampel, O. Schmitz, O. Klemp, and H. Eul (2007). Design of Sievenpiper HIS for use in planar broadband antennas by means of effective medium theory, *Advances in Radio Science*, vol. 5, pp. 87-94

- C. R. Brewitt-Taylor (2006). Limitation on the bandwidth of artificial perfect magnetic conductor surfaces," *Microwaves, Antennas & Propagation*, IET, vol. 1, pp. 255-260
- N. Guerin, S. Enoch, G. Tayeb, P. Sabouroux, P. Vincent, and H. Legay (2006). A metallic Fabry-Perot directive antenna, *Antennas and Propagation*, IEEE Trans., vol. 54, pp. 220-224
- Z. Weng, N. Wang, Y. Jiao, and F. Zhang (2007). A directive patch antenna with metamaterial structure," *Microwave And Optical Technology Lett.*, vol. 49, pp. 456
- Yuehe Ge, Karu P. Esselle, and Trevor S. Bird (2007). A High-Gain Low-Profile EBG Resonator Antenna, *Antennas and Propag. Society International Symposium*, IEEE, pp. 1301-1304
- A. Alu, F. Bilotti, N. Engheta and L. Vegni (2006). Metamaterial covers over a small aperture, *Antenna and propagation*, IEEE Trans., vol. 54, pp. 1632-1642
- Q. Wu, P. Pan, F. Y. Meng, L. W. Li, and J. Wu (2007). A novel flat lens horn antenna designed based on zero refraction principle of metamaterials, *Applied Physics A: Materials Science & Processing*, vol. 87, pp. 151-156
- J. Huang (1991). Microstrip reflectarray, *Antennas and Propagation Society International Symposium*, IEEE, pp. 612-615
- Z.H. Wu & W.X. Zhang (2005). Circularly polarized reflectarray with linearly polarized feed, *Electron. Lett.*, vol. 41, pp. 387-388
- W. Menzel, & D. Pilz (1986). Millimeter-wave folded reflector antennas with high-gain, low loss and low profile, *IEEE Antenna and Propagation Magazine*, vol. 44, pp. 24-29
- D.T. Mc Grath (1986). Planar three-dimensional constrained lens, *Antennas and Propagation*, IEEE Trans., vol. 34, pp. 46-50
- H.L. Sun, & W.X. Zhang (2007). Design of Broadband Element of Transmitarray with Polarization Trans- form, *3rd iWAT*, IEEE, Cambridge, UK, pp. 287-290
- Z.C. Ge, W.X. Zhang (2006). Broadband and high-gain printed antennas constructed from Fabry-Perot resonator structure using EBG or FSS cover, *Microwave and Optical Technology Lett.*, vol. 48, pp. 1272-1274
- R. Gardelli, M. Albani & F. Capolino (2006). Array thinning by using antennas in a Fabry-Perot cavity for gain enhancement, *Antennas and Propagation*, IEEE Trans., vol. 54, pp. 1979-1990
- A.P. Feresidis, & G. Goussetis (2005). Artificial magnetic conductor surfaces and their application to low-profile high-gain planar antennas, *Antennas and Propagation*, IEEE Trans., vol. 53, pp.209-215
- W.X. Zhang, D.L. Fu & A.N. Wang (2007). A compound printed air-fed array antenna, *Proceeding International Conference on Electromagnetics in Advanced Applications*, Torino, Italy, pp. 1054-1057

IntechOpen

IntechOpen





## **Microwave and Millimeter Wave Technologies from Photonic Bandgap Devices to Antenna and Applications**

Edited by Igor Minin

ISBN 978-953-7619-66-4

Hard cover, 468 pages

**Publisher** InTech

**Published online** 01, March, 2010

**Published in print edition** March, 2010

The book deals with modern developments in microwave and millimeter wave technologies, presenting a wide selection of different topics within this interesting area. From a description of the evolution of technological processes for the design of passive functions in millimetre-wave frequency range, to different applications and different materials evaluation, the book offers an extensive view of the current trends in the field. Hopefully the book will attract more interest in microwave and millimeter wave technologies and stimulate new ideas on this fascinating subject.

### **How to reference**

In order to correctly reference this scholarly work, feel free to copy and paste the following:

Ho-Yong Kim and Hong-Min Lee (2010). Application of Meta-Material Concepts, Microwave and Millimeter Wave Technologies from Photonic Bandgap Devices to Antenna and Applications, Igor Minin (Ed.), ISBN: 978-953-7619-66-4, InTech, Available from: <http://www.intechopen.com/books/microwave-and-millimeter-wave-technologies-from-photonic-bandgap-devices-to-antenna-and-applications/application-of-meta-material-concepts>

**INTECH**  
open science | open minds

### **InTech Europe**

University Campus STeP Ri  
Slavka Krautzeka 83/A  
51000 Rijeka, Croatia  
Phone: +385 (51) 770 447  
Fax: +385 (51) 686 166  
[www.intechopen.com](http://www.intechopen.com)

### **InTech China**

Unit 405, Office Block, Hotel Equatorial Shanghai  
No.65, Yan An Road (West), Shanghai, 200040, China  
中国上海市延安西路65号上海国际贵都大饭店办公楼405单元  
Phone: +86-21-62489820  
Fax: +86-21-62489821



© 2010 The Author(s). Licensee IntechOpen. This chapter is distributed under the terms of the [Creative Commons Attribution-NonCommercial-ShareAlike-3.0 License](https://creativecommons.org/licenses/by-nc-sa/3.0/), which permits use, distribution and reproduction for non-commercial purposes, provided the original is properly cited and derivative works building on this content are distributed under the same license.

IntechOpen

IntechOpen